AD NUMBER

AD013280

NEW LIMITATION CHANGE

TO

Approved for public release, distribution unlimited

FROM

Distribution authorized to DoD only; Administrative/Operational Use; MAY 1953. Other requests shall be referred to Office of Naval Research, One Liberty Center, Suite 1425, 875 North Randolph Street, Arlington, VA 22203-1995. Pre-dates formal DoD distribution statements. Treat as DoD

AUTHORITY

ONR ltr dtd 26 Oct 1972

AD NUMBER

AD013280

CLASSIFICATION CHANGES

TO: **unclassified**

FROM: **confidential**

LIMITATION CHANGES

TO:

Distribution authorized to DoD only; Administrative/Operational Use; MAY 1953. Other requests shall be referred to Office of Naval Research, One Liberty Center, Suite 1425, 875 North Randolph Street, Arlington, VA 22203-1995. Pre-dates formal DoD distribution statements. Treat as DoD

FROM:

Controlling DoD Organization: Office of Naval Research, One Liberty Center, Suite 1425, 875 North Randolph Street, Arlington, VA 22203-1995.

AUTHORITY

31 Dec 1953, DoDD 5200.10; Pre-dates formal DoD distribution statements. Treat as DoD only.

AD NUMBER

AD013280

CLASSIFICATION CHANGES

TO

confidential

FROM

restricted

AUTHORITY

ONR ltr dtd 11 Dec 1953

AD _____

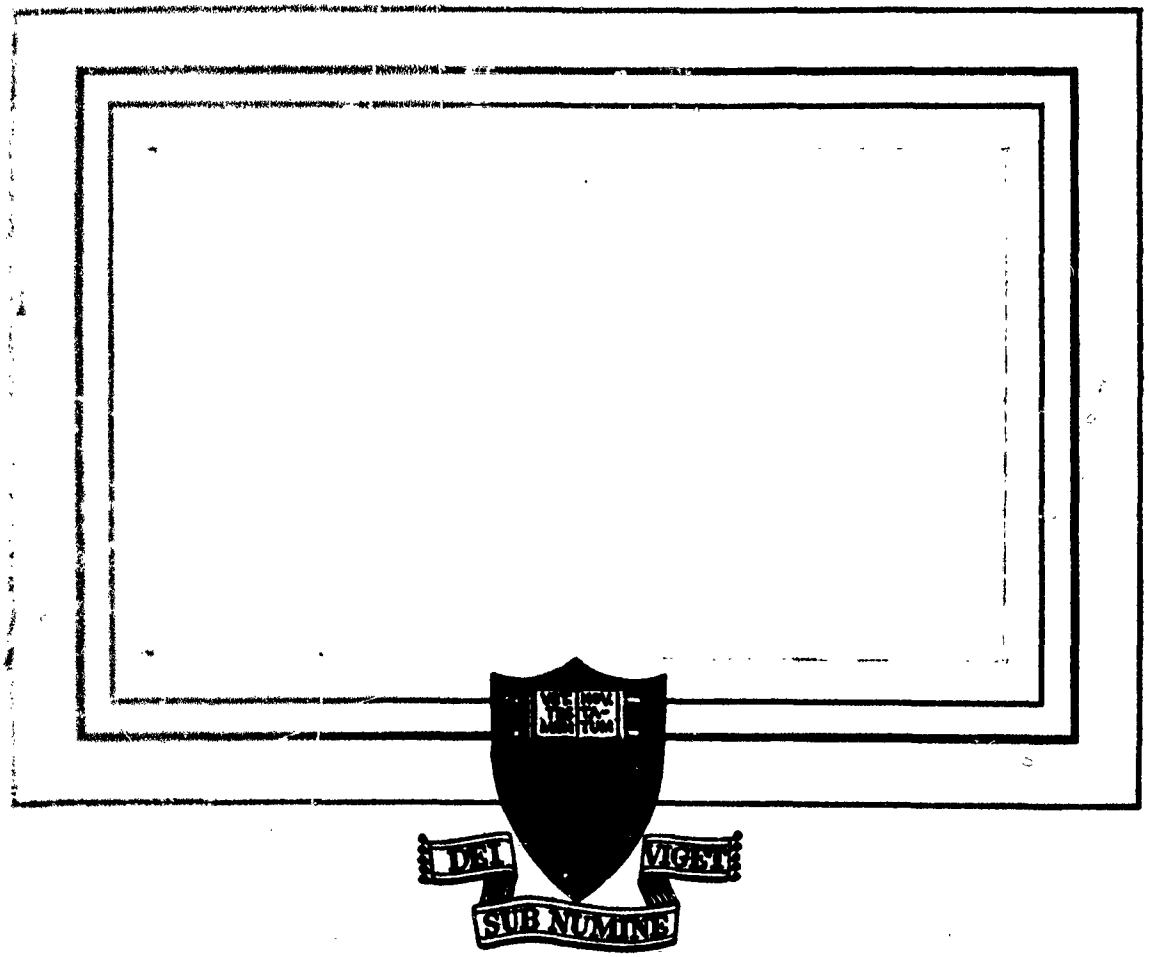

PRINCETON UNIVERSITY

DEPARTMENT OF AERONAUTICAL ENGINEERING

OFFICE OF NAVAL RESEARCH

Contract N6ori-07015

MODEL STUDY OF HELICOPTER DYNAMIC STABILITY AND CONTROL

PHASE II

COMPARISON OF THEORETICAL AND EXPERIMENTAL RESULTS NEAR HOVERING FLIGHT

Aeronautical Engineering Laboratory

Report No. 230

May, 1953

Prepared by:

R. B. GRAY

A. M. McCASKILL

D. F. GEBHARD

L. GOLAND

Approved by:

A. A. NIKOLSKY

Contents

Figures

Dynamic flight test data consisting of the response of the rotor blades and fuselage to a control step input are presented. The data were obtained by use of a helicopter model having a six-foot diameter rotor. The model has complete freedom of motion in its longitudinal plane of symmetry and is equipped with a conventional teetering rotor hub and control system.

By means of a judicious comparison of the flight test data and theoretical predictions the influence of various aerodynamic rotor parameters is evaluated. As a result, a practical method for use in hovering stability and control investigations is devised and presented (Appendix A and B).

For those concerned with model investigations a complete and detailed description of the test site, model, instrumentation, handling qualities and flight test procedures is included.

2. Introduction

The problem of stability and control has plagued helicopter development from its very beginning. It was only after numerous flight failures of rotary-wing type aircraft that the problem was fully appreciated. This problem was therefore the subject of numerous studies which attempted to explain the reasons for and the nature of the instability. In general, it was concluded that rotary-wing craft with controls fixed are inherently dynamically unstable in hovering as well as in forward flight. Nevertheless, flight was accomplished by training the pilot to deal with the instability by proper control motions. However, while it was shown that it is possible to fly the inherently unstable craft, it was soon appreciated that a more positive solution was needed. For it was evident that the pilots flying these unstable craft could not be "at ease"; they fatigued quickly due to the great concentration necessary.

The development of a helicopter which can be flown with the same ease and lack of fatigue and concentration now associated with conventional fixed-wing aircraft may take some time. However, as in the development of fixed-wing aircraft, only the simultaneous advancement of stability and control flight work with the theoretical treatment of the subject can show where improvements are to be found. While numerous theoretical treatments of the problem have been proposed, little has been accomplished to make these theories commonly accepted tools in the design of helicopters. A major reason for the disregard of such tools is the dearth of experimental data to check the accuracy and applicability of these theories. The Helicopter Laboratory at Princeton University, under the sponsorship of the Office of Naval Research, has therefore undertaken the task of furthering the engineering approach to the problem of stability and control through a simultaneous advancement of flight test work and theoretical analyses.

The increasing need for successful and economic designs of automatic pilots and control boost systems has further emphasized the necessity of such an approach. The increasing usefulness of rotary-wing aircraft for both military and civilian application certainly warrants such efforts.

At the present stage of stability and control research it would seem advisable to conduct tests utilizing full-scale helicopters. However, the vibration levels and low speeds encountered with present day helicopters have made the measurement of all the desired dynamic parameters difficult and costly. While numerous attempts have been made to obtain data from full-scale flights only limited success has been met. However, if the tests are conducted utilizing small-scale models, the following advantages can be gained:

1. Model testing can be accomplished at a fraction of the cost required for full-scale testing.

2. The problems of instrumentation, recording of test data, and test procedures are appreciably simplified.

3. To date, in published full-scale test programs, air speed could not be measured with sufficient accuracy to define the longitudinal motion (i.e. Ref. 1). However, a model may be designed so as to afford fixed references from which to measure linear and angular displacements.

4. It is relatively inexpensive to modify the construction of a model.

Consequently, after consideration of the advantages and disadvantages, a research program was initiated utilizing a semi-free flight single-rotor model. Semi-free flight refers to the fact that while the fuselage has complete freedom of motion in its longitudinal plane it is restrained in its transverse plane. This, however, does not restrict the applicability of the test results. For numerous investigators have shown, both experimentally and theoretically (i.e. Refs. 1 and 7), that the coupling between the motions in the longitudinal and transverse planes is quite loose for a single-rotor helicopter, and therefore the longitudinal oscillations may be treated independently. In addition, since the equations of motion considered actually portray the semi-free flight condition, the test results are directly applicable for use in an evaluation of these equations.

Since the primary aim of this program was to compare experimental flight test data with the corresponding theory and not to duplicate a specific helicopter, the problem of scale effect was greatly alleviated. The main scale effect would appear to be introduced in the aerodynamic characteristics of the airfoil which were readily evaluated by thrust stand tests.

3. List of Symbols

a = blade lift curve slope (per rad.)

a_1 = longitudinal inclination of tip path plane relative to X_o (rad.) (see Fig. 18)

$a_2 = \frac{1}{2}\rho bc\Omega R^2B^2$

b = number of blades

b_1 = lateral inclination of tip path plane relative to Y_o (rad.) (see Fig. 18)

$\bar{b}_0$, $\bar{b}_1$, $\bar{b}_2$, $\bar{b}_3$ = coefficients of characteristic equation

B = blade tip loss factor

B_c = control cyclic pitch angle (rad.) (see Fig. 18)

c = blade chord (ft.)

C_T = thrust coefficient $\left(\frac{T}{\pi R^2(\Omega R)^2\rho}\right)$

e = flapping hinge offset

g = gravitational acceleration (ft./sec.^{2})

h = height of rotor above helicopter center of gravity (ft.)

H_{μ_x}, H_{α_1}, etc. = coefficients of subscript terms in helicopter horizontal force equation (see Appendix A)

H_{x_o} = total force parallel to X_o axis (see Appendix C)

I_1 = blade moment of inertia about flapping axis (slug ft.^{2})

I_{y_o} = helicopter pitching moment of inertia including blades (slug ft.^{2})

k = gradient of induced velocity variation along fore and aft diameter of rotor disc. (see Appendix C)

$\bar{m}$ = total traveling mass of helicopter (slugs)

m_1 = real part of complex solution of characteristic equation

$M_{y_{\mu_x}}$, $M_{y_{\alpha_1}}$, etc. = coefficients of subscript terms in blade motion equation (see Appendix A)

$M'_{y_{\mu_x}}$, $M'_{y_{\alpha_1}}$, etc. = coefficients of subscript terms in blade motion equation (see Appendix A)

$M_{y_{o\mu_x}}$, $M_{y_{o\alpha_1}}$, etc. = coefficients of subscript terms in helicopter pitching moment equation (see Appendix A)

M_s = blade static mass moment about flapping axis (slug ft.)

n_1 = imaginary part of complex solution of characteristic equation

P_{12} = rate of change of horizontal rotor force with pitching velocity (lb. sec./rad.)

q_1 = real root of characteristic equation

Q_{11} = rate of change of horizontal rotor force with advance ratio μ_x (lb.)

r = radius of rotor blade element (ft.)

R = radius of rotor blade (ft.)

t = time from beginning of cyclic pitch disturbance (sec.)

t_1 = duration of cyclic pitch step sequence disturbance (sec.)

T = rotor thrust (lb.)

U_p = component of air velocity at blade element parallel to shaft (ft./sec.)

U_T = component of velocity at blade element perpendicular to shaft (ft./sec.)

$\bar{v}$ = mean induced velocity at rotor (ft./sec.)

v = local induced velocity at blade element (ft./sec.) (see Appendix C)

x = nondimensionalized blade element radius $(\frac{r}{R})$

$\dot{x}_o$ = longitudinal translational velocity of helicopter (ft./sec.)

X_o = longitudinal horizontal fixed coordinate (see Fig. 18)

Y_o = lateral horizontal fixed coordinate (see Fig. 18)

Z_o = vertical fixed coordinate (see Fig. 18)

α_1 = longitudinal fuselage pitch angle relative to X_o (rad.) (see Fig. 18)

β_o = rotor blade precone angle (rad.)

γ = nondimensional blade parameter $(\frac{\rho a c R^4}{I_b})$

δ = average blade drag coefficient

θ_o = blade collective pitch angle (rad.)

λ_a = mean inflow ratio $(\frac{\bar{v}}{\Omega R})$

λ_e = mean effective inflow ratio $(\frac{\bar{v}}{\Omega B R})$

μ_x = nondimensionalized translational velocity (advance ratio) $(\frac{\dot{x}_a}{\Omega R})$

ρ = air density (slugs/ft.^{3})

σ = rotor solidity $\left(\frac{bc}{\pi R}\right)$

ψ = blade azimuth angle measured from downwind position in direction of rotation (rad.)

Ω = rotor rotational velocity (rad./sec.)

4. Description of Test Equipment

The test equipment for this experimental research program consists of a completely enclosed flight space, a model helicopter with associated supporting structure and restraining mechanisms, and the required electrical and electronic equipment for measuring and recording the data.

Test Site

The flight space is completely enclosed within a brick building 28 feet wide, 17 feet high, and 58 feet long, having a lateral cross-section as shown in Fig. 1. During all test flights the model was operated at such an altitude that at no time was it close enough to any physical boundary to introduce any apparent interference effects. The control room is built into the side of the building and provides complete protection for test personnel, controls, and recording equipment. A general view of the test site is shown in Fig. 2.

The tracks upon which the model supporting system rolls are mounted on a cinder block wall at a height of four and one quarter feet above the lower level of the building. The track system is built up of extruded aluminum channel and "T" sections as shown in Fig. 3 and is so designed that both vertical and horizontal adjustments for alignment and leveling may be made by means of screws.

Elastic shock cords are stretched across and near the ends of the track to engage the model carriage and bring it to a stop if control should be lost.

Model Supporting Structure

The carriage is constructed of 24 ST extruded aluminum angle sections. It rolls on and is held on the track by means of four pairs of tall bearing rollers. One of each pair runs on top of the track; the other mounted directly below the first runs on the underside of the track. The carriage is centered on the track by four additional bearings which roll against the inside edge of the track. (See Fig. 4) The chassis of the carriage is of rectangular shape, the bearings being mounted at each corner.

Vertical freedom of motion is accomplished by allowing a square aluminum tube to move freely on four pairs of ball bearing rollers which are mounted on the superstructure of the carriage and are arranged about the tube as shown in Fig. 5 with two pairs to each set and a distance between sets of seven inches. Positive stops and elastic shock cord snubbers are built into each end of the square tube. On the upper end of the tube is mounted a yoke, also constructed of aluminum, which carries the bearings supporting the trunnions about which the model is free to pitch. The model is mounted between the trunnions in such a manner that the trunnion axis passes through the center of gravity of the model with blades. Pitch stops are attached to the yoke which limit the model pitch angle to thirty degrees in either direction. Lateral and rolling motions are completely eliminated. Fig. 6 shows the model and its supporting structure.

Model

The model is powered by a three-phase, 400 cycle, two horsepower motor. The motor is geared to the rotor shaft through a two-stage planetary gear train with a 12 to 1 speed reduction. All gears are splash lubricated with a medium light weight oil. A close-up view of the model is shown in Fig. 7. The model parameters are presented in Section 14 (pg.31).

A "teetering" type rotor is used which has two blades rigidly connected to each other through a hub. The hub is connected to the shaft by a gimbal ring which allows complete freedom in flapping about one pivot and complete freedom in cyclic feathering about the other. The blade root grips are individually pivoted for collective blade pitch angle variations.

The rotor blades are constructed of solid spruce with a one-eighth inch by three-eighths inch strip of brass buried in the leading edge so that they are balanced about their quarter chord, which is also their feathering axis. The airfoil section is a NACA 0015. The blade surface has a smooth lacquered finish.

The stabilizer bar is of the Bell type and consists of a bar with a mass on either end connected at its center to the shaft at a point below the rotor plane by a pivot whose axis is parallel to the feathering axis of the blades. The bar is further connected by suitable linkages to the blades and is free to pivot up and down while rotating. This "see-saw" motion is provided with viscous damping which determines the rate at which the motion of the bar follows the disturbed angular motion of the model shaft. The motion of the bar may introduce a cyclic variation in rotor blade angle by means of the linkages. Thus while the model is hovering, the bar is rotating in a plane perpendicular to the rotor shaft and the rotor blade angle is not affected. However, if the model is disturbed in pitch, the bar, due to gyroscopic forces, tends to remain parallel to its original plane of rotation, and hence introduces automatically a cyclic variation in blade pitch angle which tends to restore the model to its hovering condition. The main factors which affect this automatic stabilization are the viscous damping applied to the bar, the linkage ratio between the bar and the rotor, and the inertia of the bar and blades.

Viscous damping is applied to the stabilizer bar by means of a solid "swinging gate" immersed in a hemi-cyclinder of hydraulic fluid and pivoted about the axis of the cylinder. The portions of hydraulic fluid separated by the gate are connected through a passage and an adjustable needle valve. The pivot shaft of the gate is geared directly to the bar and is free to pivot as the bar does. When the model is disturbed, the bar begins to rock back and forth with respect to the rotating shaft as stated before. This movement forces the hydraulic fluid through the needle valve and results in the application of a viscous restraint to the bar. Different values of damping may be realized by adjusting the needle valve.

Model Controls

The model is completely controllable from within the control room. Rotor r.p.m. may be varied over a small range by varying the generator speed and

hence the power supply frequency. Collective and cyclic blade pitch angles are varied by means of magnetic clutches mounted on the model. Four minature magnetic clutches are employed, two for each control. The input shafts of the clutches are geared to the rotor shaft. Theoutput shafts are geared directly to a jackscrew which comprises the lower end of the corresponding blade linkage system and to a follow-up potentiometer. The manual control for each pair of magnetic clutches is an indentical potentiometer mounted in the control room. The two potentiometers of each control are so connected electrically that a movement of the control potentiometer introduces an error signal which by means of an electronic amplifier causes one of the pair of clutches to engage, thus running the jackscrew up or down and rotating the follow-up potentiometer so as to cancel out the error signal and disengage the clutch. A cyclically varying blade pitch angle is introduced through a swashplate which may be tilted by the jackscrew about an axis parallel to the fuselage pitch axis only. Collective blade pitch angles are introduced by moving the swash plate and linkages vertically along the rotor shaft.

A view of the model and control room is shown in Fig. 6. Fig. 8 shows the control panel.

Instrumentation

The model and carriage are instrumented to record the following data: vertical and horizontal displacements, vertical and horizontal accelerations, fuselage pitching angle, fuselage pitching angular acceleration, rotor flapping angle with respect to the rotor shaft, collective blade pitch angle, cyclic blade pitch angle, rotor shaft speed, and the drag of the mechanical servo carriage carrying the trailing cables.

Vertical and horizontal displacements are recorded by means of a series of electrical contacts mounted on the track and on the square tube. As the model moves vertically or horizontally, insulated leaf springs mounted on the carriage brush these contacts and close the circuit, thus allowing an electrical pulse to flow in the circuit which may be recorded by an oscillograph. The amplitude and polarity of the pulses vary from contact to contact in a preset manner so that they form a pattern on the oscillograph record. A reversal of direction reverses the order in which the contacts are made, and hence the pattern on the record. Reversal in direction and the displacement at which it occurs is thereby easily determined.

A minature accelerometer of range $\pm$ 1.5g is mounted on the vertical tube to generate a signal for the recording of vertical accelerations. A similar accelerometer is mounted on the carriage for horizontal accelerations.

Fuselage pitching angle is recorded by means of a potentiometer which is driven by a spur gear mounted on the model pitch shaft. Both rotor blade and stabilizer bar flapping are recorded in a similar manner. An angular accelerometer is mounted on the fuselage pitch axis to measure fuselage pitching angular accelerations. (See Fig. 7)

Collective and cyclic blade pitch angle are recorded as an oscillograph galvanometer deflection proportional to the change in resistance from the center terminal to an outside terminal of their respective follow-up potentiometers.

Rotor shaft speed is obtained by recording an electrical pulse introduced by the opening of a set of breaker points by a cam mounted on the rotor shaft.

A visual indication of rotor speed is obtained for the operator by measuring the output voltage of a small d.c. generator mounted on the bottom of the motor case and driven at motor shaft speed.

Drag of the mechanical servo carriage is measured by a strain gage beam. This circuit, as well as the accelerometer circuits and the rotor flapping circuit have electrical filters included to reduce the hash level. All data are recorded by a Heiland Type A 301R Oscillograph.

Cable Carriage

Since the power lines, controls, and instrumentation require a large number of shielded, insulated wires to be trailed from the model, a means of reducing the drag on the model of this multi-conductor cable was devised. It consists of an endless motor-driven steel cable as a power source, two block friction clutches mounted on a lead carriage, and a number of smaller carriages to support the cable. (See Fig. 6) The motor-driven cable is mounted on pulleys outside of and a few inches below the level of the track and completely encircles the track. The friction clutches are mounted on levers on the lead carriage, with one on either side of the track in a position to engage the steel cable. The remaining carriages are placed on the tracks and are fastened at intervals to the trailing multi-conductor cable, supporting its weight and allowing it to hang in loops between them. The model carriage is connected to the friction clutch levers so that a relative movement between this carriage and the lead cable carriage engages one of the friction clutches depending upon the direction of movement. These clutches then assume a great portion of the multi-conductor cable drag, inertia, and carriage friction (the amount being proportional to the ratio of the lever arms which in this case is about 95%) and the cable is pulled along the track with only a small effect on the over-all model motion. The force exerted by the cable carriage upon the model was found to be in phase with the model translational acceleration (Fig. 16). It is conservatively estimated that this force effectively increases the translational mass of the model by a maximum of 2.5 percent.

5. Flight Test Procedure

Before attempting any flight tests a static thrust stand analysis of the model was made. The model was installed on the thrust stand and the blade linkages were adjusted until the blades were "in track." Collective blade pitch angle was then reduced until zero thrust was reached. The rotor was stopped and the blade root angle was measured. This blade root angle was then used as a reference for succeeding measurements. Measurements of thrust and torque were taken for various collective blade pitch angles with the rotor speed being held constant.

During the first familiarization flights, the stabilizer bar damping was kept at a low value to help the pilot keep the model under control. However as the pilot became more adept at anticipating the model motion and response to the control movements, it was found that the model could be kept under control and could be maneuvered about as desired with the stabilizer bar locked out completely, although the model was unstable in this condition. It was rather quickly established after several losses of control and near accidents that to keep the model under control required the utmost concentration and a continual movement of the controls. The pilot, having to substitute the sense of sight for the helicopter pilot's sense of feel of the helicopter movement, could not remove his sight from the model long enough to do anything more than glance at the instruments. This resulted in noticeable mental fatigue and physical tenseness after a few moments flight. After more flight experience was gained, it was found that the model could be allowed to go out of control and then control could be rather quickly established although the amount, direction, and timing of control application were very critical, especially the direction and timing. Further flight experience allowed the pilot to fly the model in a more peaceful frame of mind though the visual concentration and continual movement of the controls were required with the resulting fatigue. In spite of this, it was decided to test this unstable configuration for two reasons. One, it resulted in larger displacements for a given disturbance which reduced the percentage reading error, and two, it removed the added complications of including the effect of the stabilizer bar in the theory and data reduction.

The flight test procedure, as planned, required that the model be disturbed from a steady hovering flight condition and the resulting motion recorded. As intimated in the preceding paragraph, a steady hover was not easily realizable. It was comparatively easy to keep the model in one position on the track due to the slight friction in the carriage bearings, but it was very difficult to stop all motion about the pitching axis. It was found that the motion resulting from an introduced disturbance was extremely sensitive to initial pitching motions. Usually, unless the model was exactly hovering, no more than half a cycle of disturbed motion could be recorded before the model engaged one of the safety stops. However when great care was taken to hover the model, it was found that a large amplitude, unstable motion would build up from zero, and as many as five or six complete cycles could be observed and recorded.

The realization of an exact steady hover required the utmost concentration by the pilot and a continual slight movement of the controls. It appeared to be more a matter of luck than skill. Much time was consumed in attempting to

attain this condition and when realized, it appeared to last only for an instant of time, which resulted in many false starts. It should perhaps be noted that the response of the model helicopter to a control motion or a disturbance is much faster than that of a full scale machine.

The test procedure was then as follows. The test equipment was first inspected and the instrumentation checked out. Then, with the oscillograph and instrumentation on stand-by, the model was brought up to speed and an attempt was made to hover it as described above. When it was thought that this was accomplished, the oscillograph was started and a predetermined disturbance was applied to the rotor by introducing an error signal into the cyclic pitch circuit. The oscillograph recorded the resulting motion until the model engaged one of the stops. The oscillograph record was then developed and the data analyzed.

Three special tests were made in an effort to determine the model stability derivatives by restricting the model motion. In the first test, the model was locked in pitch and in horizontal displacement. Then, with the model hovering, a cyclically varying blade pitch angle was introduced and the resulting blade flapping motion was recorded by the oscillograph.

For the second test, the model was locked in pitch but was free in horizontal displacement. Then, starting from the hovering condition, the model was pulled along the track and the blade flapping motion due to forward velocity was recorded by the oscillograph.

For the third test, the model was locked in horizontal displacement and a spring force proportional to angular displacement was introduced about the pitching axis. Then, starting again from the hovering condition, the model was disturbed and the resulting oscillatory fuselage pitching and rotor flapping motions were recorded.

6. Precision of Measurements

It is conservatively estimated that the data as read from the oscillograph records have the following tolerances:

Linear Displacements	$\pm$ 1/32 inch
Linear Acceleration	$\pm$ .01 foot/sec.^{2}
Pitching Angles	$\pm$ .003 radian
Pitching Acceleration	$\pm$ .02 radian/sec.^{2}
Collective and Cyclic Blade Pitch Angles	$\pm$ .002 radian
Total Blade Flapping Angles	$\pm$ .003 radian
Blade Flapping Phase Angle	$\pm$ 10°
Rotor Angular Velocity	$\pm$ 3.5%
Trailing Cable Drag	$\pm$ .02 lb.
Time	$\pm$ .002 second

Horizontal velocity and fuselage pitching velocity were determined by fitting a curve to the faired displacement data and then differentiating this expression. It is estimated that the tolerances are of the order of $\pm$ 0.3 foot/sec. and $\pm$ .008 radian/sec. respectively. The rotor angular velocity tolerance as given above is based on the measurement of any one revolution. If two or three consecutive revolutions are taken, the possible error can be greatly reduced.

Since the rotor instrumentation measures the total flapping angle with respect to the shaft, the determination of the longitudinal and lateral components depends to a great degree on the accuracy of the value of the blade flapping phase angle. Since it was impossible to measure the angle within 10°, the percentage error in determining values of the component blade flapping angles, velocities, and accelerations may be quite large, especially at phase angles near 0° and 90°.

7. Discussion of Test Results

The results of the thrust stand tests of the model are presented in Figs. 9 and 10. Fig. 9 is a plot of thrust coefficient versus blade collective pitch angle. Also presented is a comparison with the theory of Ref. 2 for a lift curve slope of 5.75 per radian. Fig. 10 shows the variation of rotor profile drag coefficient with blade collective pitch for a three-quarter radius Reynolds Number of 313,000 and was calculated from thrust stand torque data, again using the theory of Ref. 2. As pointed out in Section 8, both of these parameters must be accurately determined, either experimentally or theoretically, for the stability theory to closely predict the actual helicopter motion.

A typical oscillograph record is presented as Fig. 11, while Figs. 12 thru 15 show a direct comparison between theory and experiment for the fuselage pitching motion and horizontal velocity response due to a cyclic pitch step disturbance. There was no measurable change in rotor r.p.m. during the test runs. In order to obtain theoretical curves including the effects of linear and static friction it was found convenient to use an analog computer. Equations A-1 thru A-4 (Appendix A) were therefore modified to include friction terms, and terms involving $\dot{b}_1$ and $\ddot{b}_1$ were neglected (as discussed in Appendix A) as being small. The fuselage pitch angle (α_1) and horizontal velocity ($\dot{x}_o$) responses were then obtained for an input similar to that used to excite the model.

It can be seen from Figs. 12 thru 15 that the experimental values of fuselage pitch angle and horizontal velocity are in good agreement with the theoretical values for the first cycle of oscillation. During this time the model exhibits a slight divergence with a period of oscillation of 7.1 seconds. After the first cycle agreement is not as good. This is believed to be the result of the cumulative effects of random servo carriage drag (Section 4), random changes in friction forces, and recirculation. The difference between the curves of exact theory and quasi-static theory (Fig. 14) is due primarily to the presence of friction terms in the former curve which could not be easily introduced into the quasi-static calculations.

The blade flapping motion, as recorded by the oscillograph during a run, did not give particularly good agreement with the theoretically predicted motion. While the phase angle between the tip path plane motion and the fuselage degrees of freedom agreed with theory, the amplitude of the motion was greater than theory would predict.

To gain an insight into the flapping motion an attempt was made to determine the longitudinal and lateral components of flapping due to forward velocity independently from the other rotor derivatives. For this purpose the model was restrained from pitching, hovered at one end of the track, and then manually moved along the track at varying velocities and the resulting blade motion measured. The range of velocities covered was from zero to about eight feet per second. This corresponds roughly to the range encountered in the flight tests of the model.

The resulting plot (Fig. 17) of longitudinal and lateral components of flapping against tip speed ratio, μ_x, reveals a scatter of points varying as much as four or five tenths of a degree. Part of this scatter can be

attributed to reading accuracy (Section 6), but it must be assumed that the greater part of the scatter is indicative of the actual blade motion. For verification of this assumption a series of tests was made in which the model was restrained from moving in a translational sense in addition to having any pitching motion eliminated. The cyclic pitch was then varied over a range of five degrees and the blade flapping motion measured. For this test also the same order of magnitude of scatter was apparent and seemed to be independent of flapping amplitude. This seems to indicate that, if the former tests could be run at velocities high enough to make the scatter small in comparison with the total flapping, experimental values for the rotor velocity derivatives could be obtained. This was not feasible with the existing experimental setup. The tests did indicate, however, (Fig. 17) that the longitudinal flapping due to forward velocity was at least of the order of magnitude predicted by theory, and that the lateral flapping due to forward velocity also gives agreement if a linear induced velocity variation with forward velocity is assumed as discussed in Appendix C.

In another direct attempt at measuring stability derivatives the model was locked in horizontal displacement and restrained about the pitching axis by a known spring force. The fuselage pitching and blade flapping motions were then measured after the model had been disturbed from its hovering flight condition. Unfortunately the reduction of data from this test required a greater accuracy of blade flapping measurement than that obtainable with the present instrumentation, and therefore no concrete results were obtained. However, an attempt will be made in the near future to remedy this situation through use of larger displacements and greater measurement accuracy so as to obtain the individual rotor derivatives.

8. Effect of Various Aerodynamic Parameters

The determination of the actual blade collective pitch is of extreme importance in the accurate prediction of stability and control characteristics. For example, an error of ten percent in blade angle can produce a discrepancy of the same order of magnitude in the period of oscillation. The simplest and most common method of obtaining this parameter in the absence of measured flight test values is by use of the simple momentum theory which is based upon a constant induced velocity distribution of the magnitude

$$v = \sqrt{\frac{T}{2\rho\pi R^2 B^2}}$$

The collective blade angle can then be determined from blade element theory

$$T = \frac{1}{2}\rho b c a \Omega^2 R^3 \int_0^B x^2 \left(\theta_0 + \frac{\lambda_a}{x}\right) dx$$

where $\lambda_a = -v/\Omega R$. However such an approach gives an erroneous value for this parameter. For example, this method applied to the test model gives a value of $\theta_0 = 10.2^\circ$ which does not compare satisfactorily with the measured value of $\theta_0 = 9.1^\circ$. Consequently, basing stability and control characteristics upon this approach results in an appreciable error.

For the tests described in this report the collective blade angle was determined from static thrust stand tests (Fig. 9). However it was found that the method of Ref. 2, which is based upon a more exact theory than that described above, accurately predicts these values, and therefore in the absence of measured flight test values its use is recommended. Fig. 9 shows the agreement between thrust stand tests and the theory of Ref. 2 for the test model. Once the collective pitch has been determined, the problem of induced velocity distribution arises again in the prediction of the helicopter motion. While Ref. 2 permits a rather exact distribution to be computed, such a downwash variation is quite difficult to incorporate into a stability and control analysis. Although a triangular distribution along the blade approximates the actual distribution in hovering flight for most helicopters, it was found that, once the collective blade angle is known, an assumption of a constant downwash distribution along the blade (based on the actual θ_0) results in only a small error. In addition, since the more exact triangular distribution had little effect upon the resulting motion, and since such an assumption made it difficult to incorporate any increase in downwash from the front to the rear of the rotor disc at small forward velocities, the assumption of constant downwash at zero forward velocity was retained. The consideration of a change in induced velocity distribution across the disc with forward velocity is essential to a prediction of lateral flapping. However it should be noted that this latter consideration does not affect the period or damping of the longitudinal motion nor does it affect the control response. Thus if the lateral blade motion is of little interest, the assumption of a constant downwash (based on the actual collective pitch) in or near hovering flight appears to give good results.

The assumption has been made for the purposes of this work that the profile drag coefficient along the blade is a constant. This greatly simplifies the analysis of the problem and appears to be a good assumption. Several calculations were made to determine the effect of an error in the mean profile

drag coefficient upon the helicopter motion. It was found that an error of ten percent in the determination of the profile drag coefficient could result in an error of about one percent in the period of oscillation of the helicopter. Small errors in profile drag therefore will not appreciably alter the results of the stability analysis.

The neglect of the blade tip loss appears to be one of the least valid of the assumptions previously made in stability analyses. The simplification which such an assumption enables is not great, and the error involved can be considerable. Calculations indicate that for the model helicopter under consideration, assuming the tip loss factor equal to unity instead of a theoretical value of

$$B = 1 - \frac{\sqrt{2C_T}}{b}$$ (Appendix A)

can result in an error in the period of oscillation of the order of fifteen percent.

9. Conclusions and Recommendations

Dynamic flight test data consisting of the response of the rotor blades and fuselage to a control input have been presented. By means of a judicious comparison of the flight test data and theoretical predictions the influence of various aerodynamic rotor parameters has been evaluated. In part, it has been found that the determination of the actual blade collective pitch angle and the consideration of blade tip loss effects are essential to an accurate prediction of stability and control characteristics.

A practical hovering stability and control method of investigation has been devised (Appendix A and B). The experimental fuselage pitch and translational velocity responses have been shown to be in good agreement with that predicted by the above method. Due to difficulties encountered in the measurement of blade flapping only qualitative correlation of the blade motions could be obtained.

The effects of rotor downwash in disturbed motion have been dealt with herein in an approximate manner. It is therefore recommended that continued effort be expended in the determination of this phenomenon to thereby check the applicability of the method adopted herein.

Finally it can be stated that this initial program in addition to yielding valuable flight test data has demonstrated that model testing affords a ready means of investigating helicopter dynamics.

10. Appendix A

Method for Stability and Control Analysis

The following analysis is, in most respects, similar to that presented by Nikolsky in Ref. 4. However, in the light of the discussions of Section 8 presented herein, certain modifications, principally concerned with the determination of the hovering collective pitch angle and downwash, are made. The method is briefly discussed below. For a detailed account of the theory use of the above reference is recommended.

Coordinate Axes

The coordinate axes for this analysis are illustrated in Fig. 18. The origin is at the center of the rotor hub, and the Z_o axis is the gravity axis. The X_o axis and Y_o axis are in the longitudinal and lateral planes of the helicopter respectively when it is in the initial hovering position. These coordinates are fixed in space and all translational and angular displacements are relative to them.

Assumptions

1. All displacements are assumed small. The usual small angle assumptions, i.e., $\sin \alpha_1 = \alpha_1$, $\cos \alpha_1 = 1$, are therefore applicable.

2. The center of gravity of the helicopter is on the rotor axis.

3. The effects of blade taper and built in twist may be accounted for by using a mean square chord and an average collective pitch angle, each calculated from performance theory.

4. The induced velocity is constant over the disc, and the tip loss effect may be accounted for by using an effective aerodynamic rotor radius, BR, as subsequently evaluated. This radius is used in all terms except those involving inertia effects; i.e., blade flapping moment of inertia, blade static moment, etc., which are obviously based on the geometric and mass properties of the blades.

5. The blades and control system are assumed to be infinitely stiff. The validity of this assumption depends upon the aerodynamic, elastic, and inertial properties of the blades and the control system. The effect of blade flexibility and unbalance is treated in Ref. 5, while the effect of control system flexibility is dealt with in Ref. 6. This assumption is valid for blades that are both mass and aerodynamically balanced and have a stiff control system.

6. The effects of reversed flow, motion about the drag hinge, and the fuselage drag and moment are considered negligible.

7. The profile drag coefficient is constant along the blades.

8. The rotor r.p.m. is contant.

9. The lateral and longitudinal modes of oscillation are effectively uncoupled.

Equations of Motion

Four equations may be written in terms of α_1, μ_x, a_1, and b_1. The first two equations are obtained by summing the horizontal forces and the pitching moments about the helicopter c.g., and the last two are obtained by equating the blade airload moments to the inertia moments about the flapping hinge and equating coefficients of like trigonometric terms.

The equation summing the horizontal forces may be expressed as,

$$H_{\dot{\mu}x}\dot{\mu}_x + H_{\mu x}\mu_x + H_{\ddot{\alpha}_1}\ddot{\alpha}_1 + H_{\alpha_1}\alpha_1 + H_{\dot{a}_1}\dot{a}_1 + H_{a_1}a_1 + H_{\dot{b}_1}\dot{b}_1 + H_{b_1}b_1 = H_{B_c}B_c \qquad \text{(A-1)}$$

Similarly, the equation summing the pitching moments about the c.g. is

$$M_{y_0\mu x}\mu_x + M_{y_0\ddot{a}_1}\ddot{a}_1 + M_{y_0\alpha_1}\alpha_1 + M_{y_0\ddot{a}_1}\ddot{a}_1 + M_{y_0\dot{a}_1}\dot{a}_1 + M_{y_0 a_1}a_1 + M_{y_0\dot{b}_1}\dot{b}_1 + M_{y_0 b_1}b_1 = M_{y_0 B_c}B_c \qquad \text{(A-2)}$$

The equations for the blade motion are:

$$M_{y\dot{\mu}x}\dot{\mu}_x + M_{y\mu x}\mu_x + M_{y\ddot{a}_1}\ddot{a}_1 + M_{y\dot{a}_1}\dot{a}_1 + M_{y\dot{b}_1}\dot{b}_1 + M_{yb_1}b_1 = 0 \qquad \text{(A-3)}$$

$$M'_{y\mu x}\mu_x + M'_{y\alpha_1}\alpha_1 + M'_{y\dot{a}_1}\dot{a}_1 + M'_{ya_1}a_1 + M'_{y\ddot{b}_1}\ddot{b}_1 + M'_{y\dot{b}_1}\dot{b}_1 = B_c \qquad \text{(A-4)}$$

where (Ref. 4),

$$H_{\dot{\mu}x} = \Omega RB\overline{m}$$

$$H_{\mu x} = \frac{a_2\Omega RB}{2}\left(\delta + \frac{aB_0^2}{2} - a\theta_0\lambda_e\right)$$

$$H_{\ddot{\alpha}_1} = -\overline{m}h$$

$$H_{\alpha_1} = \frac{aa_2\lambda_e\Omega RB}{4}$$

$$H_{\dot{a}_1} = -\frac{aa_2B_0RB}{6}$$

$$H_{a_1} = \frac{aa_2\Omega RB\lambda_e}{4} + T$$

$$H_{\dot{b}_1} = -\frac{a_2a\overline{RB}}{2}\left(\frac{\theta_0}{3} + \lambda_e\right)$$

$$H_{b_1} = \frac{-aa_2\Omega RBB_0}{6}$$

$$H_{B_c} = \frac{-aa_2\lambda_e\Omega RB}{4}$$

$$M_{y\mu_x} = \frac{eb}{8}\left(c\rho a B_0 \Omega^2 R^3 B^3\right) + h H_{\mu_x}$$

$$M_{y\ddot{\alpha}_1} = I_{y_0}$$

$$M_{y\alpha_1} = eb\left(\frac{M_s \Omega^2}{2}\right) + Th + H_{\alpha_1}$$

$$M_{y\ddot{a}_1} = -eb\,\frac{M_s}{2}$$

$$M_{y\dot{a}_1} = -\frac{eb}{12}\left(\rho a c \Omega R^3 B^3\right) + h H_{\dot{a}_1}$$

$$M_{ya_1} = eb\left(\frac{M_s \Omega^2}{2}\right) + h H_{a_1}$$

$$M_{y b_i} = -eb M_s \Omega + h H_{b_i}$$

$$M_{y b_1} = -\frac{eb}{12}\left(\rho a c \Omega^2 R^3 B^3\right) + h H_{b_1}$$

$$M_{y\beta} = h H_\beta$$

$$M_{y\dot{\mu}_x} = -\frac{8 B_0 M_s R B}{\gamma \Omega I_1}$$

$$M_{y\mu_x} = -\frac{4}{3} B_0$$

$$M_{y\ddot{a}_1} = \frac{8}{\gamma \Omega^2}$$

$$M_{y\dot{a}_1} = \frac{1}{\Omega}$$

$$M_{y b_i} = \frac{16}{\gamma \Omega}$$

$$M_{y b_1} = 1.0$$

$$M'_{y\mu_x} = a\left(\frac{4}{3}\theta_0 + \lambda_e\right)$$

$$M'_{y\alpha_1} = -1.0$$

$$M'_{y\dot{a}_1} = -\frac{16}{\gamma \Omega}$$

$$M'_{ya_1} = -1.0$$

$$M'_{y b_i} = \frac{8}{\gamma \Omega^2}$$

$$M'_{y b_1} = \frac{1}{\Omega}$$

Calculations based on the above equations are long and complicated, and it has been found desirable to utilize certain characteristics of the helicopter motion to simplify the analysis. For example, it has been shown (Ref. 7) that the blade flapping oscillation relative to the shaft is heavily damped and of a much higher frequency than the divergent fuselage oscillation. Consequently, in investigating the long period divergent fuselage oscillation, the rather high frequency, damped oscillation of the blades may be neglected. This is equivalent to discarding blade inertial terms $\ddot{a}_1$ and $\ddot{b}_1$ in the above blade equations. Sissingh (Ref. 8) has demonstrated that the criteria for the above assumption is that the blade inertia number γ be greater than $60n_1/\Omega$, which is generally true for conventional helicopters. This is equivalent to the requirement that the blade flapping motion damp to 1/10 amplitude within 1/10 of the fuselage oscillation period.

Furthermore, Hohenemser (Ref. 9) has shown that for a conventional helicopter, the amplitude of the tip path plane motion relative to the shaft is small compared to the amplitude of the fuselage pitching motion. Thus, the tip path plane pitching velocity may be approximated by the fuselage pitching velocity (i.e. $\dot{a}_1 = -\dot{\alpha}_1$) with little loss in accuracy. Similarly the magnitudes of all the b_1 terms, and the μ_x term in eq. (A-3), are small and may be neglected.

Making these simplifications and neglecting flapping hinge offset, equations (A-3) and (A-4) may be solved for a_1 and b_1 and the results placed in equations (A-1) and (A-2) to yield,

$$\Omega R \overline{m} \mu_x + Q_{11} \mu_x - h \overline{m} \ddot{\alpha}_1 + P_{12} \dot{\alpha}_1 - T\alpha_1 = T B_c \qquad \text{(A-5)}$$

$$h Q_{11} \mu_x + I_{y_0} \ddot{\alpha}_1 + h P_{12} \dot{\alpha}_1 = T h B_c \qquad \text{(A-6)}$$

The above solution is referred to as a "quasi-static" solution since it represents the condition in which the angle of the tip-path plane at any instant is dependant solely on α_1, $\dot{\alpha}_1$, and μ_x.

There are now only two aerodynamic terms in the equations: Q_{11}, the rate of change of horizontal force with advance ratio (translational velocity), and P_{12}, the rate of change of horizontal force with pitching velocity.

The translational velocity term may be written in terms of collective pitch angle and effective inflow ratio as follows,

$$Q_{11} = \frac{\rho a b c \Omega^2 R^3 B^3}{36}\left[\frac{9\delta}{a} + \frac{\theta_0^2}{2} + 39\theta_0\lambda_e + 16\theta_0^2 + 27\lambda_e^2\right] \qquad \text{(A-7)}$$

The pitching velocity term may also be written in terms of collective pitch angle and effective inflow ratio.

$$P_{12} = \frac{4\Omega b I_1}{RB}\left(\frac{2\theta_0}{3} + \frac{3\lambda_e}{2}\right) \qquad \text{(A-8)}$$

As mentioned in Section 8 of this report the accuracy with which the collective pitch angle is determined is very important, and the simplifying assumption of constant induced velocity should only be made once the collective pitch angle has been accurately predicted.

Knowing the collective pitch angle, the effective inflow ratio λ_e may be calculated.

$$\lambda_c = \frac{4C_T}{a\sigma B^3} - \frac{2\theta_a}{3} \qquad \text{(A-9)}$$

where the tip loss factor from Ref. 4 is

$$B = 1 - \frac{\sqrt{2C_T}}{b} \qquad \text{(A-10)}$$

Characteristic Equation

When the Laplace transforms of equations (A-5) and (A-6) are written in determinant form and expanded, the characteristic equation becomes

$$\bar{b}_3\lambda^3 + \bar{b}_2\lambda^2 + \bar{b}_1\lambda + \bar{b}_0 = 0 \qquad \text{(A-11)}$$

where

$$\bar{b}_3 = 1$$

$$\bar{b}_2 = \frac{h R_\theta}{I_{y_0}} + \left(\frac{1}{m} + \frac{h^2}{I_{y_0}}\right)\frac{Q_{11}}{\Omega R B}$$

$$\bar{b}_1 = 0$$

$$\bar{b}_0 = \frac{hg\,Q_{11}}{I_{y_0}\Omega R B}$$

For the conventional helicopter the real root of the above equation describes a highly damped convergence while the complex roots describe the fuselage period of oscillation and rate of divergence.

Response to a Step Disturbance Sequence

Writing the complete expansion of the determinant form of equations (A-5) and (A-6) for the fuselage pitch response from an initial hovering condition,

$$\frac{\alpha(\Delta)}{\theta_c} = \frac{(h/I_{y_0})T\Delta}{\lambda^3 + \bar{b}_2\lambda^2 + \bar{b}_0} - \frac{(h/I_{y_0})T\Delta e^{-\lambda(t-t_1)}}{\lambda^3 + \bar{b}_2\lambda^2 + \bar{b}_0} \qquad \text{(A-12)}$$

where t_1 is the duration of the step disturbance, and the second term is used only after the step disturbance sequence has been completed.

If the roots of the characteristic equation are represented as

$$\lambda_1 = q_1$$

$$\lambda_2 = m_1 \pm in_1$$

the response may be written

$$\frac{\alpha_1}{\theta_c} = \frac{(h/I_{y_0})T\theta_a e^{q_1 t}}{3q_1^2 + 2b_2 q_1} + \frac{2(h/I_{y_0})T\theta_a e^{m_1 t}}{\sqrt{C_1^2 + D_1^2}}\sin\left[nt + \tan^{-1}\frac{C_1}{D_1}\right] \qquad \text{(A-13)}$$

before the step disturbance sequence has been completed and

$$\frac{\alpha}{\beta_c} = \frac{(h/I_{y_o})T(e^{q_1 t} - e^{q_1(t-t_1)})}{3q_1^2 + 2\bar{b}_2 q_1} + \frac{2(h/I_{y_o})T}{\sqrt{C_1^2 + D_1^2}}\left\{e^{m_1 t}\sin\left[n_1 t + \tan^{-1}\frac{C_1}{D_1}\right] - e^{m_1(t-t_1)}\sin\left[n_1(t-t_1) + \tan^{-1}\frac{C_1}{D_1}\right]\right\} \quad \text{(A-14)}$$

after the step disturbance sequence has been completed, where

$$C_1 = 3(m_1^2 - n_1^2) + 2\bar{b}_2 m_1$$

$$D_1 = 6m_1 n_1 + 2\bar{b}_2 n_1$$

The translational velocity response may be similarly determined and expressed as follows

$$\frac{\dot{x}_e}{\beta_c} = \frac{T^2 h}{\bar{b}_0 \bar{m} I_{y_o}} + \frac{[T(I_{y_o} + h^2\bar{m})q_1^2 + T^2 h]e^{q_1 t}}{q_1(3q_1^2 + 2\bar{b}_2 q_1)\bar{m} I_{y_o}} + \frac{2\sqrt{X_e^2 + Y_e^2}\, e^{m_1 t}}{\bar{m} I_{y_o}(m_1^2 + n_1^2)(C_1^2 + D_1^2)}\sin\left[n_1 t + \tan^{-1}\frac{X_e}{Y_e}\right] \quad \text{(A-15)}$$

before the step disturbance sequence has been completed and

$$\frac{\dot{x}_e}{\beta_c} = \frac{[T(I_{y_o} + h^2\bar{m})q_1^2 + T^2 h]e^{q_1(t-t_1)}}{q_1(3q_1^2 + 2\bar{b}_2 q_1)\bar{m} I_{y_o}} + \frac{2\sqrt{X_e^2 + Y_e^2}}{\bar{m} I_{y_o}(m_1^2 + n_1^2)(C_1^2 + D_1^2)}\left\{e^{m_1 t}\sin\left[n_1 t + \tan^{-1}\frac{X_e}{Y_e}\right] - e^{m_1(t-t_1)}\sin\left[n_1(t-t_1) + \tan^{-1}\frac{X_e}{Y_e}\right]\right\}$$

after the step disturbance sequence has been completed, where C_1 and D_1 are defined, as above and

$$X_e = A_1 C_1 m_1 + B_1 D_1 m_1 + B_1 C_1 n_1 - A_1 D_1 n_1$$

$$Y_e = A_1 C_1 n_1 + B_1 D_1 n_1 - B_1 C_1 m_1 + A_1 D_1 m_1$$

$$A_1 = T(I_{y_o} + h^2\bar{m})(m_1^2 - n_1^2) + T^2 h$$

$$B_1 = 2T(I_{y_o} + h^2\bar{m})m_1 n_1$$

These pitching and translational responses are compared with the experimental results in Fig. 14.

11. Appendix B

Typical Application of Method

The model helicopter described in Section 14 (pg. 31) of this report will be analyzed by the method of Appendix A.

Calculation of the thrust coefficient at sea level yields,

$$C_T = \frac{T}{\pi R^2 (\Omega R)^2 \rho} = .00391$$

The tip loss factor then may be obtained from eq. A-10.

$$B = 1 - \frac{\sqrt{2C_T}}{b} = .956$$

The collective pitch angle is determined from Ref. 2, or experimentally (Fig. 9), and the effective inflow ratio is calculated from eq. A-9.

$$\theta_0 = .159 \text{ radians}$$

$$\lambda_c = \frac{4C_T}{a\sigma B^3} - \frac{2\theta_0}{3} = -.0351$$

The values of Q_{11} and P_{12} are calculated from eqs. A-7 and A-8.

$$Q_{11} = \frac{\rho a b c \Omega^2 R^3 B^3}{36}\left[\frac{9\delta}{a} + \frac{\theta_0^2}{2} + 39\theta_0\lambda_c + 16\theta_0^2 + 27\lambda_c^2\right]$$

$$= 13.9$$

$$P_{12} = \frac{4\Omega b I_1}{RB}\left(\frac{2\theta_0}{3} + \frac{3\lambda_c}{2}\right) = 1.37$$

The coefficients of the characteristic eq. A-11 can now be evaluated.

$$\bar{b}_2 = \frac{hP_{12}}{I_{y_0}} + \left(\frac{1}{m} + \frac{h^2}{I_{y_0}}\right)\frac{Q_{11}}{\Omega RB} = 6.60$$

Since in this case, the model translating mass is not equal to the lifted mass, i.e., $\bar{m} \neq T/g$, $\bar{b}_0$ must be modified to equal,

$$\bar{b}_0 = \frac{hQ_{11}T}{I_{y_0}\Omega RBm} = 4.694$$

The characteristic equation is therefore

$$\lambda^3 + 6.60\lambda^2 + 4.694 = 0$$

and the roots of this equation are,

$$g_1 = -6.705$$

$$m_1 + i n_1 = .0525 \pm .84\, i$$

Therefore, the period of oscillation is

$$\frac{2\pi}{.84} = 7.47 \text{ seconds}$$

and the increase in amplitude in the first half period = $e^{\frac{(.0525)(7.47)}{2}}$ = 1.217. The fuselage pitch response to a .65 second cyclic pitch step disturbance can be calculated from eq. A-13 and A-14 as follows:

$$C_1 = 3(m_1^2 - n_1^2) + 2\bar{b}_2 m_1 = -1.416$$

$$D_1 = 6 m_1 n_1 + 2\bar{b}_2 n_1 = 11.36$$

For $0 < t < .65$

$$\frac{\alpha_1}{B_c} = \frac{(h/I_{y_a})T e^{g_1 t}}{3g_1^2 + 2\bar{b}_2 g_1} + \frac{2(h/I_{y_a})T e^{m_1 t}}{\sqrt{C_1^2 + D_1^2}} \sin\left[n t + \tan^{-1}\frac{C_1}{D_1}\right]$$

$$= 3.45 e^{-6.705 t} + 27.95 e^{.0525 t} \sin[.84 t - .1240]$$

For $t \geq .65$

$$\frac{\alpha_1}{B_c} = \frac{(h/I_{y_a})T(e^{g_1 t} - e^{g_1 (t-.65)})}{3g_1^2 + 2\bar{b}_2 g_1} + \frac{2(h/I_{y_a})T}{\sqrt{C_1^2 + D_1^2}}$$

$$\left\{e^{m_1 t} \sin\left[n_1 t + \tan^{-1}\frac{C_1}{D_1}\right] - e^{m_1 (t-.65)} \sin\left[n_1 (t-.65) + \tan^{-1}\frac{C_1}{D_1}\right]\right\}$$

$$= 3.45 e^{-6.705 t}\left[1 - e^{4.36}\right] + 27.95 e^{.0525 t}\left\{\sin(.84 t - .1240)\right.$$

$$\left. - e^{.0341} \sin(.84 t - .6700)\right\}$$

The translational velocity response to a .65 second cyclic pitch step disturbance may be similarly calculated from eq. A-15.

For $0 < t < .65$

$$\frac{\dot{x}_a}{B_c} = 859.3 - 38.85 e^{-6.705 t} + 811.2 e^{.0525 t} \sin(.84 t - 1.51)$$

For $t \geq 2.65$

$$\frac{\dot{z}_g}{U} = 38.85\, e^{-6.705t}\left[1 - e^{4.36}\right] + 811.2\, e^{.0525t}$$
$$\left\{\sin(.84t - 1.511) - e^{.084}\sin(.84t - 2.056)\right\}$$

The above pitching and translational velocity responses are compared with experimental results in Fig. 14.

12. Appendix C

Consideration of Linear Induced Velocity Variation with Forward Velocity

It is generally believed that as the helicopter enters forward flight the induced velocity over the rear of the rotor disc is greater than that over the forward portion. If the downwash is assumed to increase linearly from the front to the rear of the rotor disc, its magnitude at any point can be expressed as

$$v = \bar{v}(1 + k x \cos\psi)$$

where $\bar{v}$ is the mean induced velocity and k is the gradient of induced velocity variation along the fore and aft diameter of the rotor disc. The normal velocity at a blade element can then be written

$$U_p = (\Omega r b_1 + r\dot{a}_1 - \beta_0 \dot{x}_0 + \lambda_a \Omega + k)\cos\psi + (-r\Omega a_1 + r b_1)\sin\psi + \lambda_a \Omega R$$

Substituting this expression into the rotor longitudinal force equation (Ref. 4 - pg. 192).

$$H_{x_0} = \frac{1}{2\pi}\int_0^{2\pi} d\psi \int_0^R \frac{1}{2}\rho b c \left\{ U_T^2 \delta \sin\psi - a(\theta U_T^2 + U_P U_T)\left[(\beta_0 - a_1\cos\psi - b_1\sin\psi)\cos\psi + \frac{U_P}{U_T}\sin\psi\right]\right\} dr$$

and integrating gives an additional longitudinal force term

$$\Delta H_{x_0} = -\frac{1}{2}\rho b c \Omega R^2 \left[\frac{a\beta_0 \lambda_a \Omega k R}{6}\right]$$

For very near hovering flight Ref. 3 gives a gradient of

$$k = -.5\,\frac{\mu_x}{\lambda_a}$$

Under such a linearization the change in horizontal force is a function of forward velocity, and the rate of change of longitudinal force with tip speed ratio becomes

$$H_{\mu_x} = \frac{a_2 \Omega R B}{2}\left(\delta + \frac{a\beta_e^2}{2} - a\theta_0\lambda_e + \frac{a\beta_0}{6}\right)$$

instead of the value given in Appendix A. In a similar manner, the new value for the rate of change of lateral flapping with tip speed ratio becomes

$M_{\mu_x} = -\frac{1}{3}\beta_0 - \frac{1}{2}$

The incorporation of these new derivatives into the helicopter equations of motion results in no change in the longitudinal response but gives better correlation between theoretical and experimental results for lateral flapping near hovering flight.

13. References

1. Stewart, W., "Flight Testing of Helicopters," The Journal of the Royal Aero. Society, May, 1948.

2. Castles, Walter, and Ducoffe, Arnold, "Static Thrust Analysis for Helicopter Rotors and Airplane Propellers," Journal of the Aeronautical Sciences, May, 1948.

3. Coleman, R. P., Feingold, A. M., and Stempin, C. W., "Evaluation of the Induced Velocity Field of an Idealized Helicopter Rotor," NACA ARR No. L5E10, June, 1945.

4. Nikolsky, A. A., "Helicopter Analysis," Chapt. 6, John Wiley and Sons, Inc., 1951.

5. Goland, Leonard, "The Effects of Rotor Blade Flexibility and Unbalance on Helicopter Hovering Stability and Control," Princeton University Aero. Eng. Report No. 218, Feb., 1953.

6. McCaskill, Allan M., "The Effects of Viscous and Elastic Control System Restraints on Helicopter Hovering Stability and Control," Princeton University Aero. Eng. Report No. 223, March, 1953.

7. Miller, R. H., "Helicopter Control and Stability in Hovering Flight," Journal of the Aeronautical Sciences, August, 1948.

8. Sissingh, G. J., "Comparison of Helicopter Rotor Model Tests of Aerodynamic Damping with Theoretical Estimates," A. R. C. Technical Note Aero. 2118, August, 1951.

9. Hohenemser, K., "Dynamic Stability of a Helicopter with Hinged Rotor Blades," Ingenieur-Archiv, Vol. 9, pp. 419-428, December, 1938 (NACA T. M. No. 907, 1938).

14. Table of Model Parameters

No. of blades, $b = 2$

Blade radius, $R = 3$ ft.

Rotor angular velocity, $\Omega = 120.4$ rad./sec.

Solidity, $\sigma = .0441$

Blade chord, $c = .208$ ft.

Blade airfoil section - NACA 0015

Slope of lift curve, $a = 5.75$/rad.

Average blade profile drag coefficient, $\delta = .0244$

Collective pitch angle, $\theta_o = .159$ rad.

Blade moment of inertia, $I_1 = .077$ slug. ft.^{2}

Blade static moment, $M_s = .0385$ slug ft./blade

Precone angle, $\beta_o = .0436$ rad.

Height of rotor above model center of gravity, $h = .96$ ft.

Blade loading factor, $C_T/\sigma = .0887$

Lifted weight, $T = 34.36$ lbs.

Total traveling mass, $\bar{m} = 1.364$ slugs

Model mass moment of inertia including blades, $I_{y_o} = .206$ lb. ft. sec.^{2}

Model center of gravity is on the shaft axis.

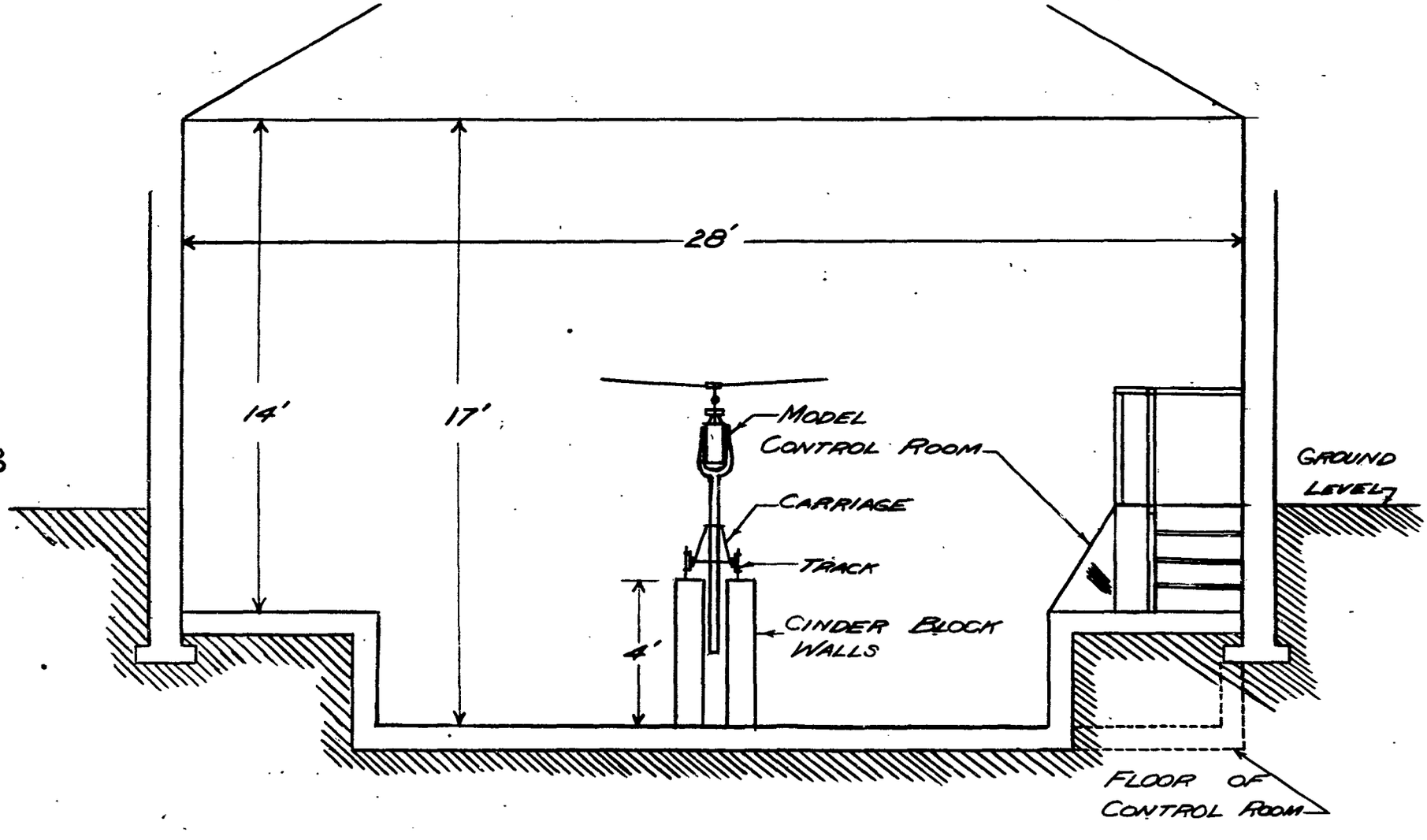

Fig. 1 Lateral Cross Section of Test Site

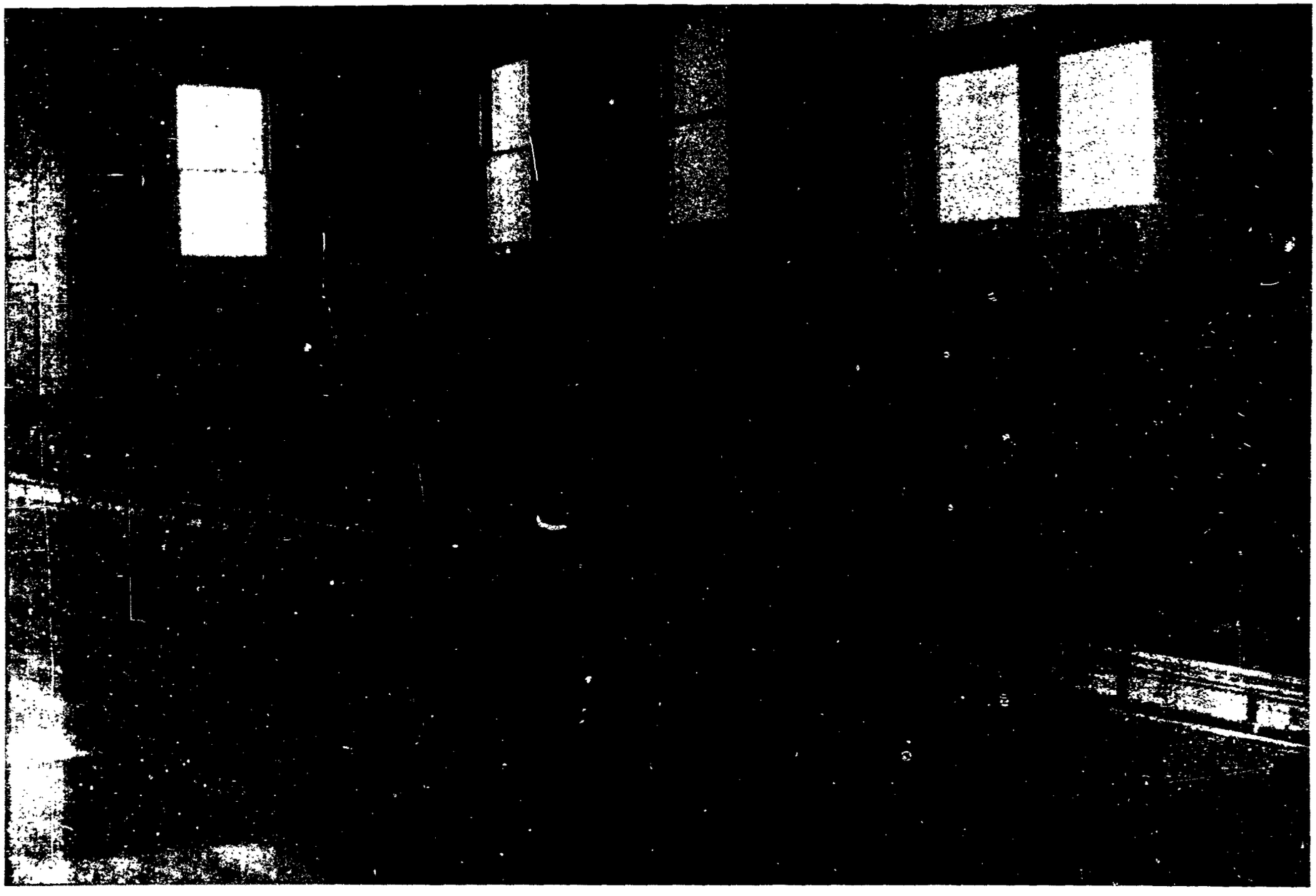

Fig. 2 A General View of Test Site and Model

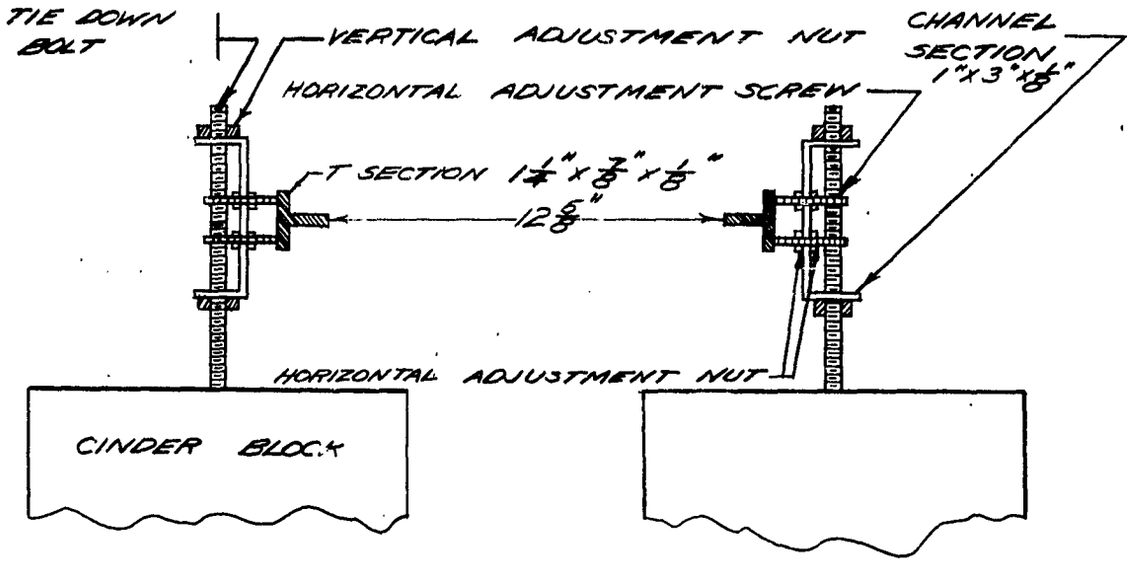

Fig. 3 Track Cross Section

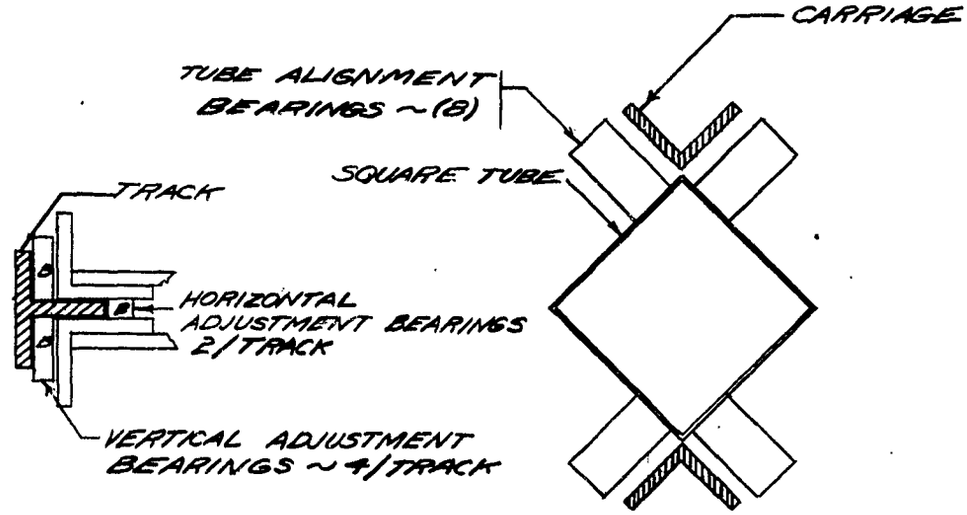

Fig. 4 Layout of Carriage Bearings

Fig. 5 Layout of Tube Bearings

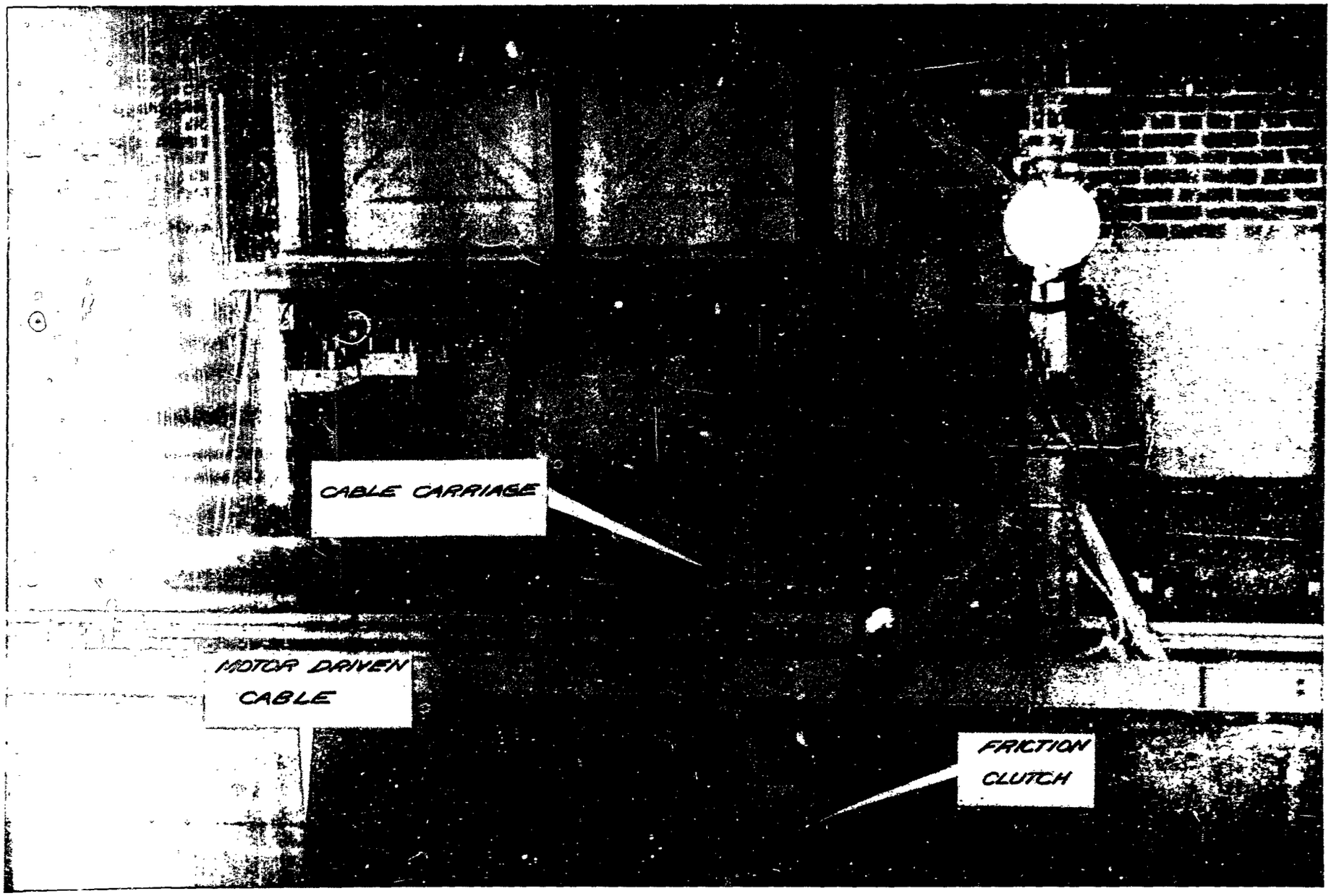

Fig. 6 Model, Cable Carriage, Supporting Structure, and Control Room

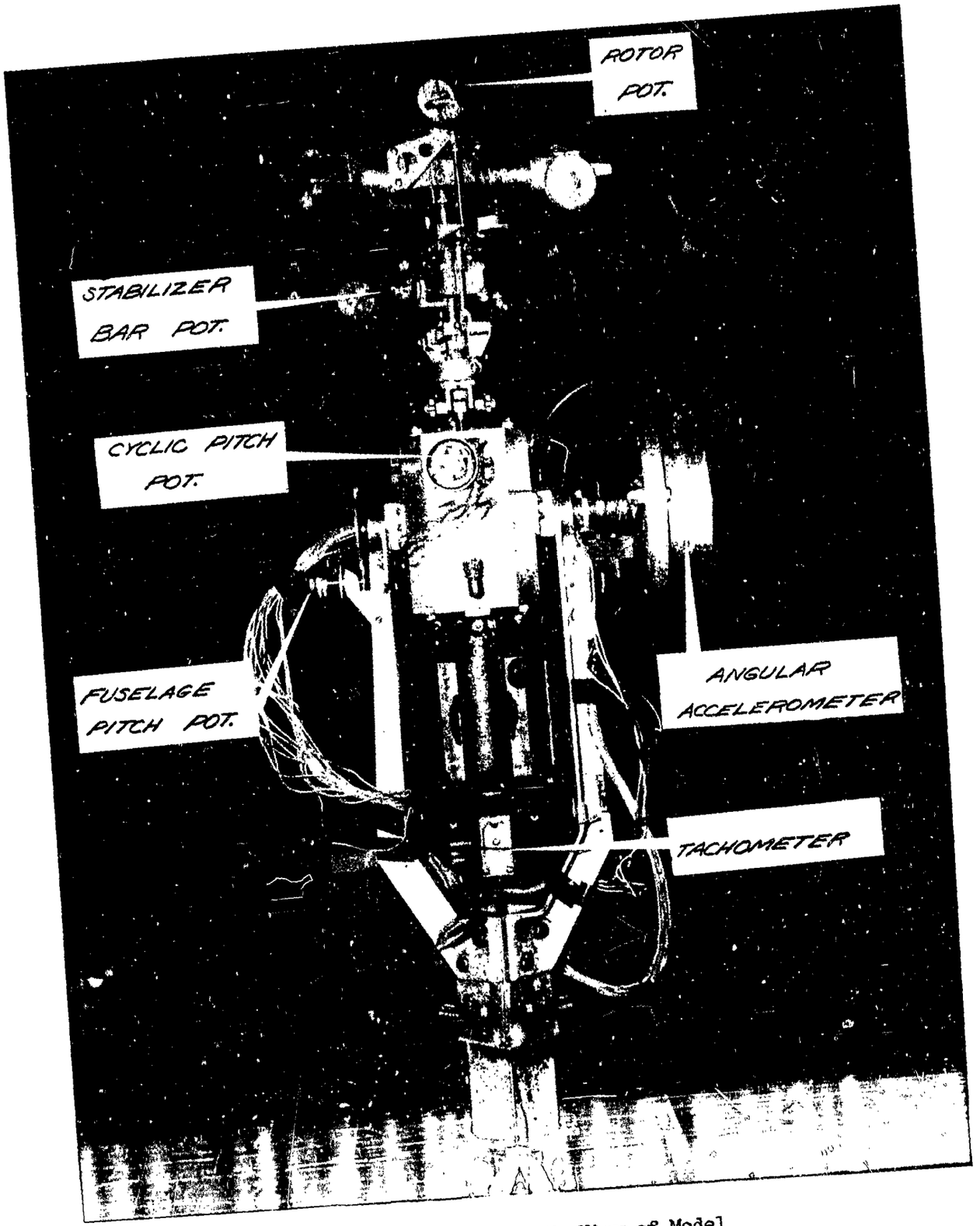

Fig. 7 Close-Up View of Model

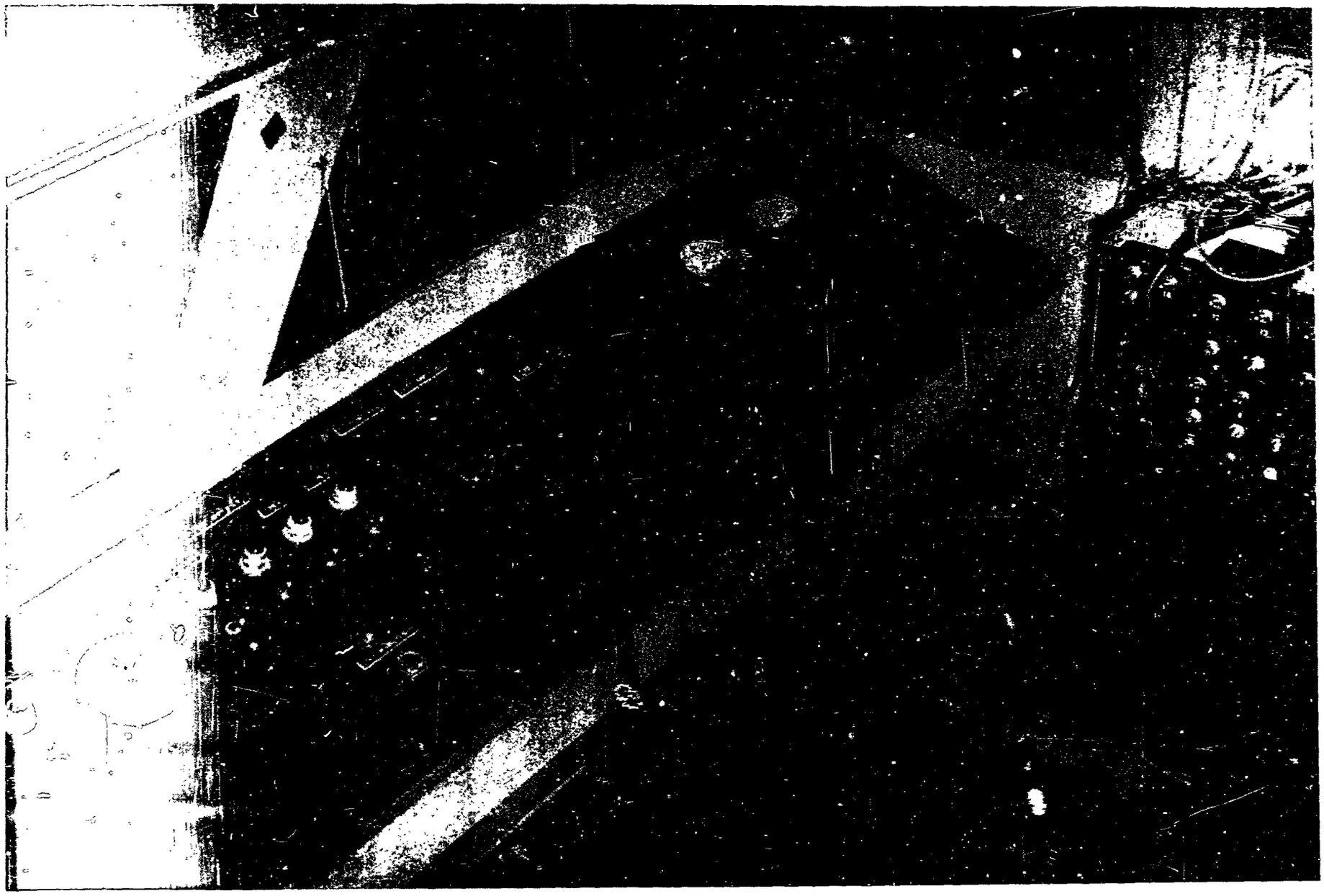

Fig. 8 View of Control Panel

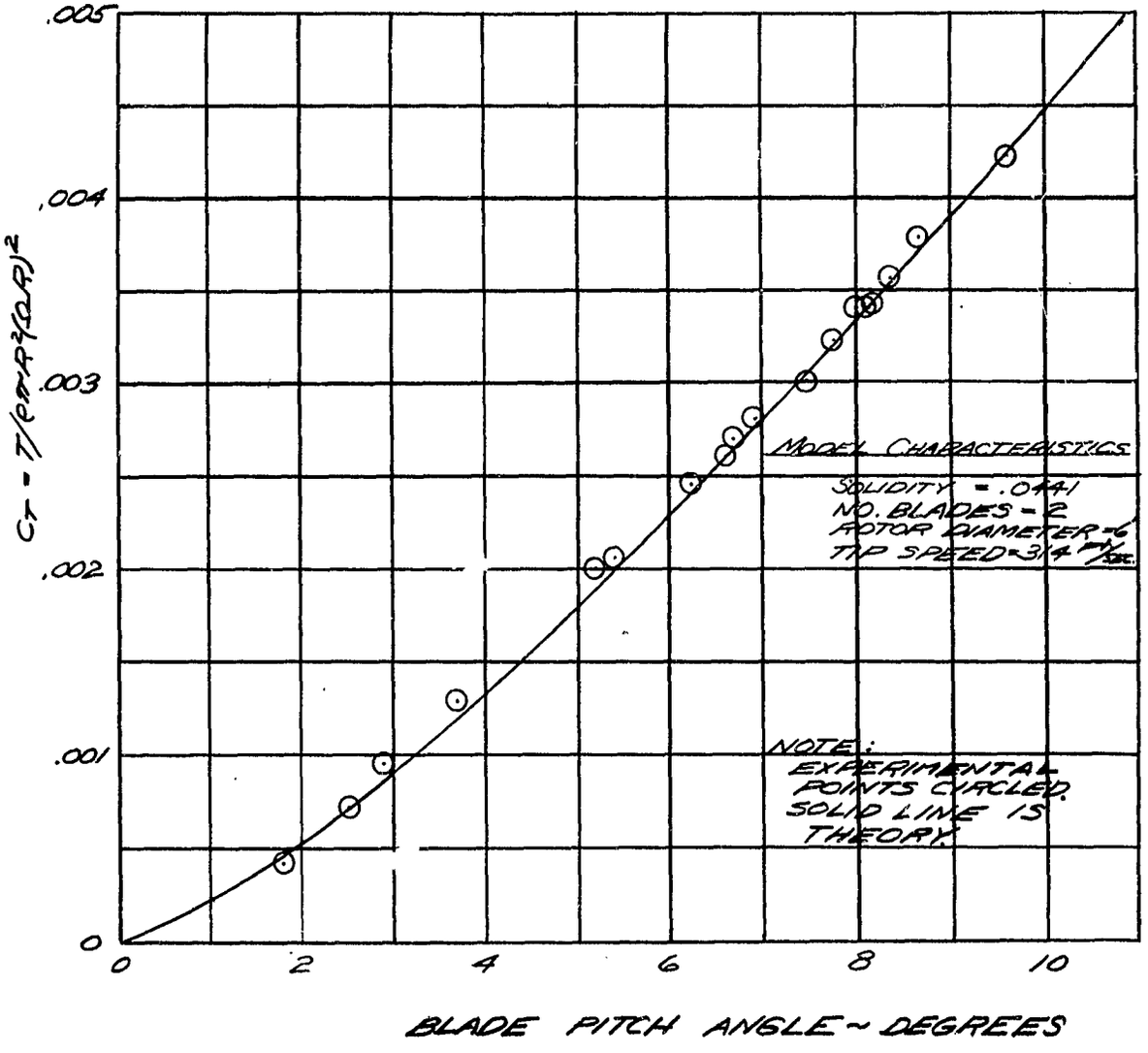

Fig. 9 Thrust Stand Data - C_T vs. θ_o

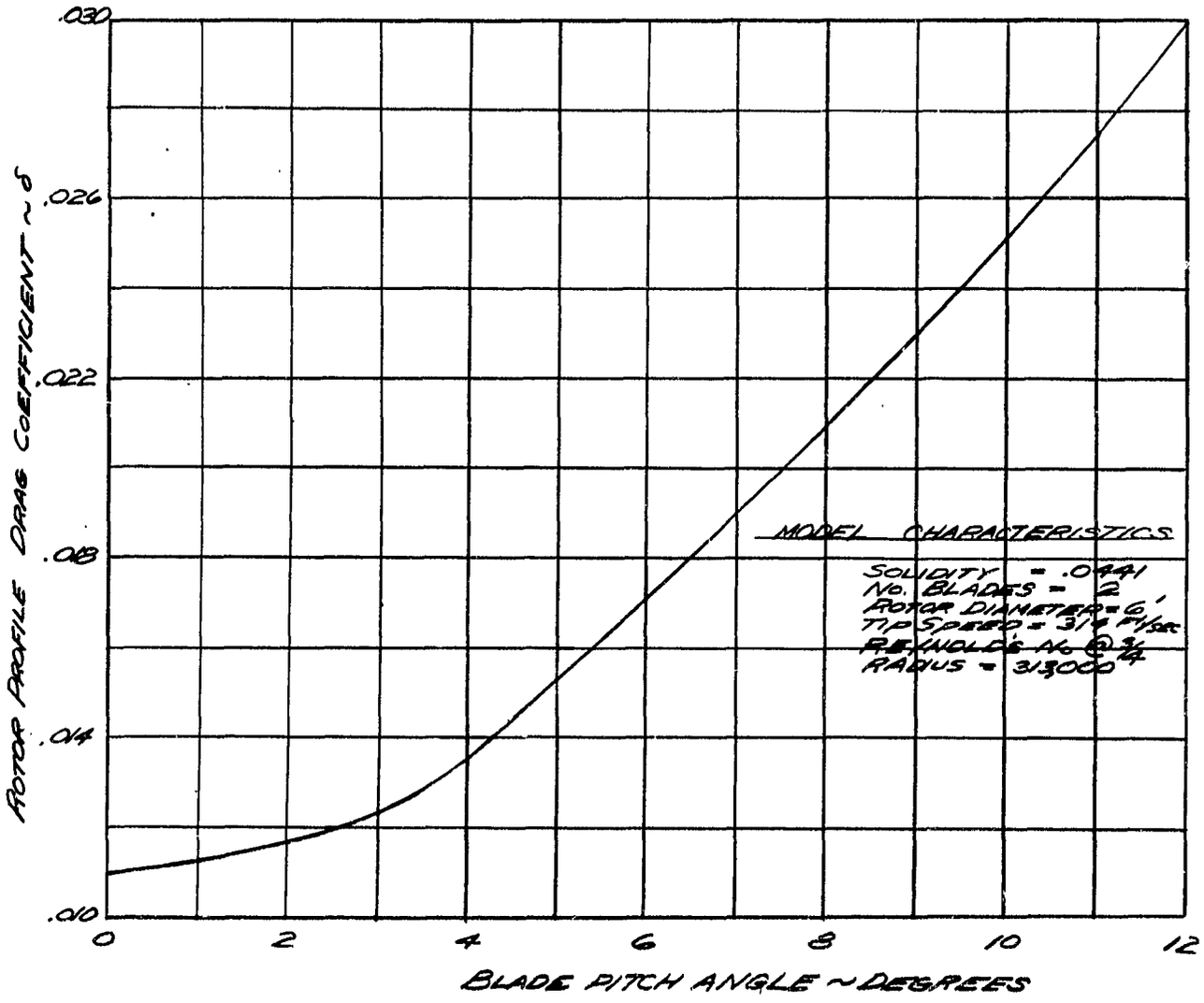

Fig. 10 Thrust Stand Data - δ vs. Θ_0

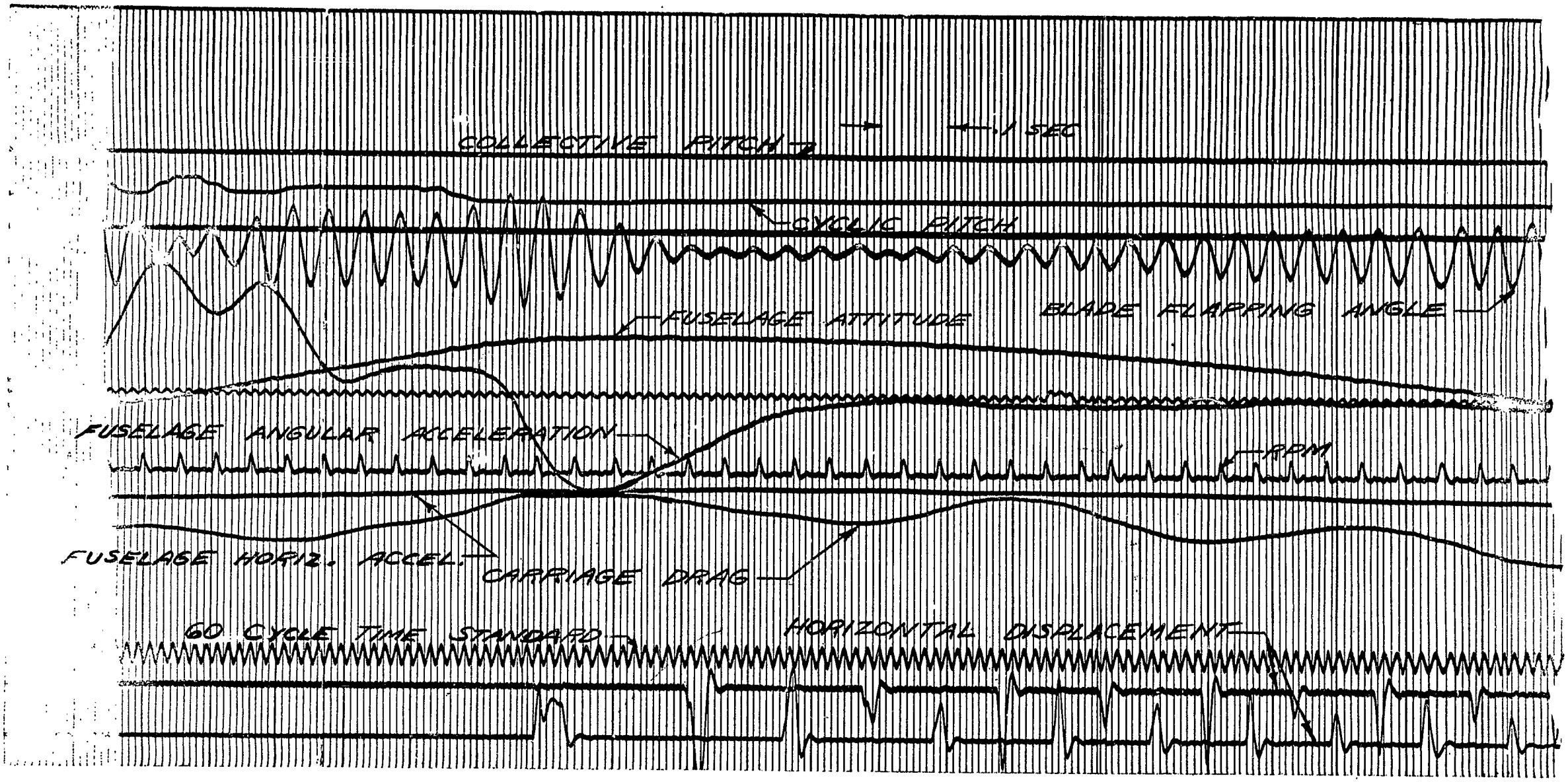

Fig. 11 Typical Oscillograph Record

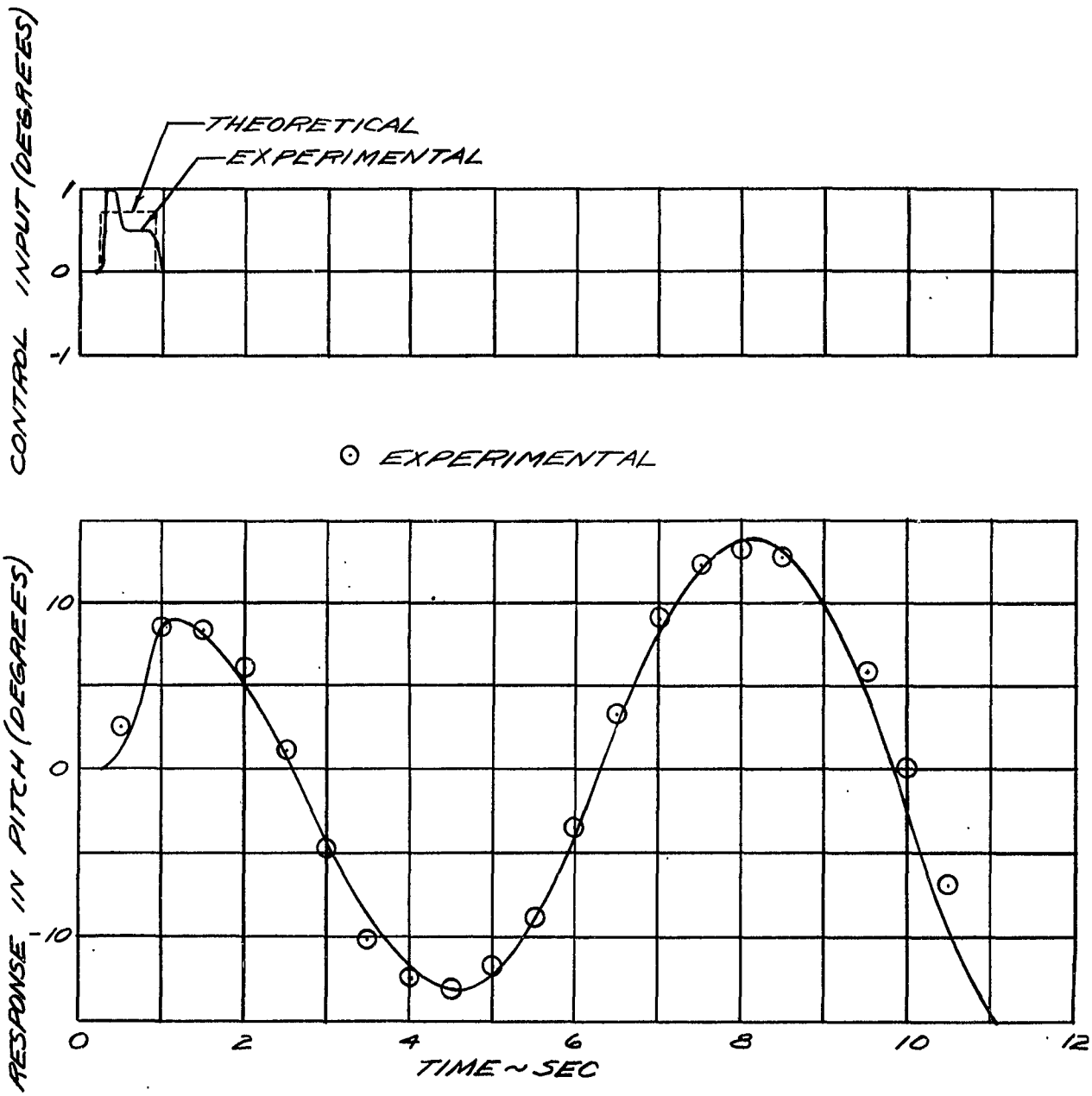

Fig. 12. Experimental and Theoretical Fuselage Response to a Step Disturbance - (Run 2-9-53)

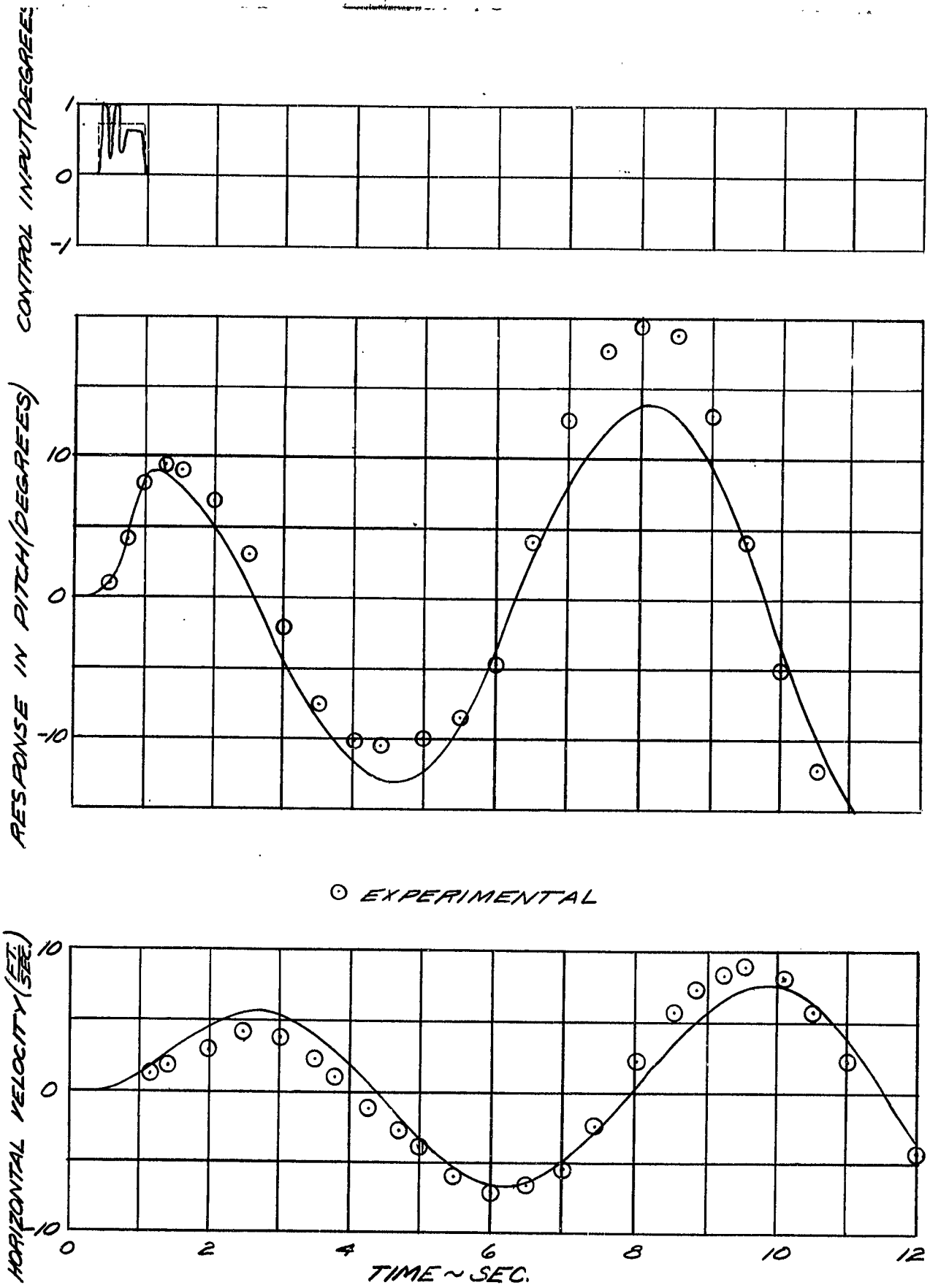

Fig. 13 Experimental and Theoretical Fuselage Response to a Step Disturbance - (Run 2-10-53)

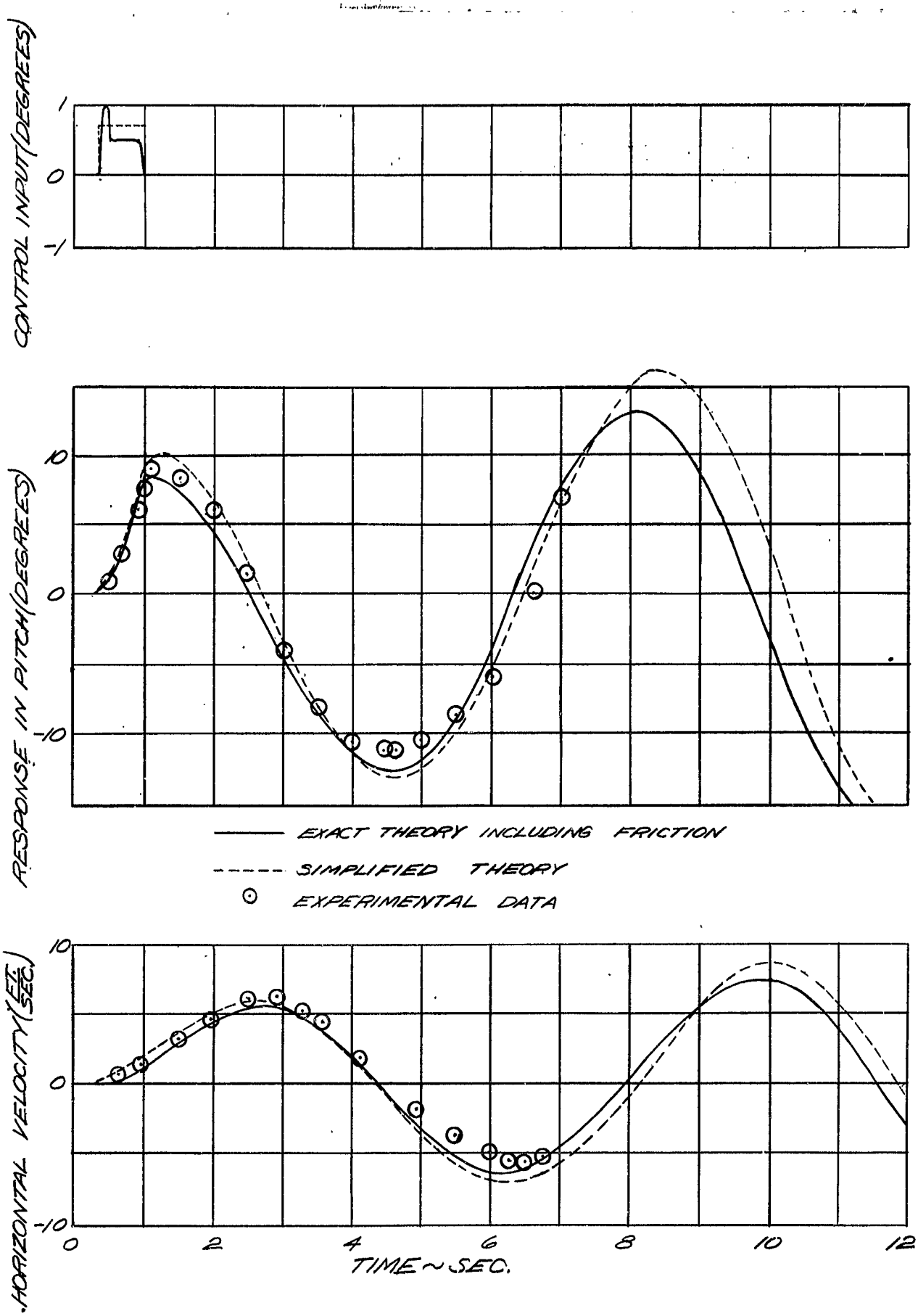

Fig. 14 Experimental and Theoretical Fuselage Response to a Step Disturbance - (Run 2-18-53)

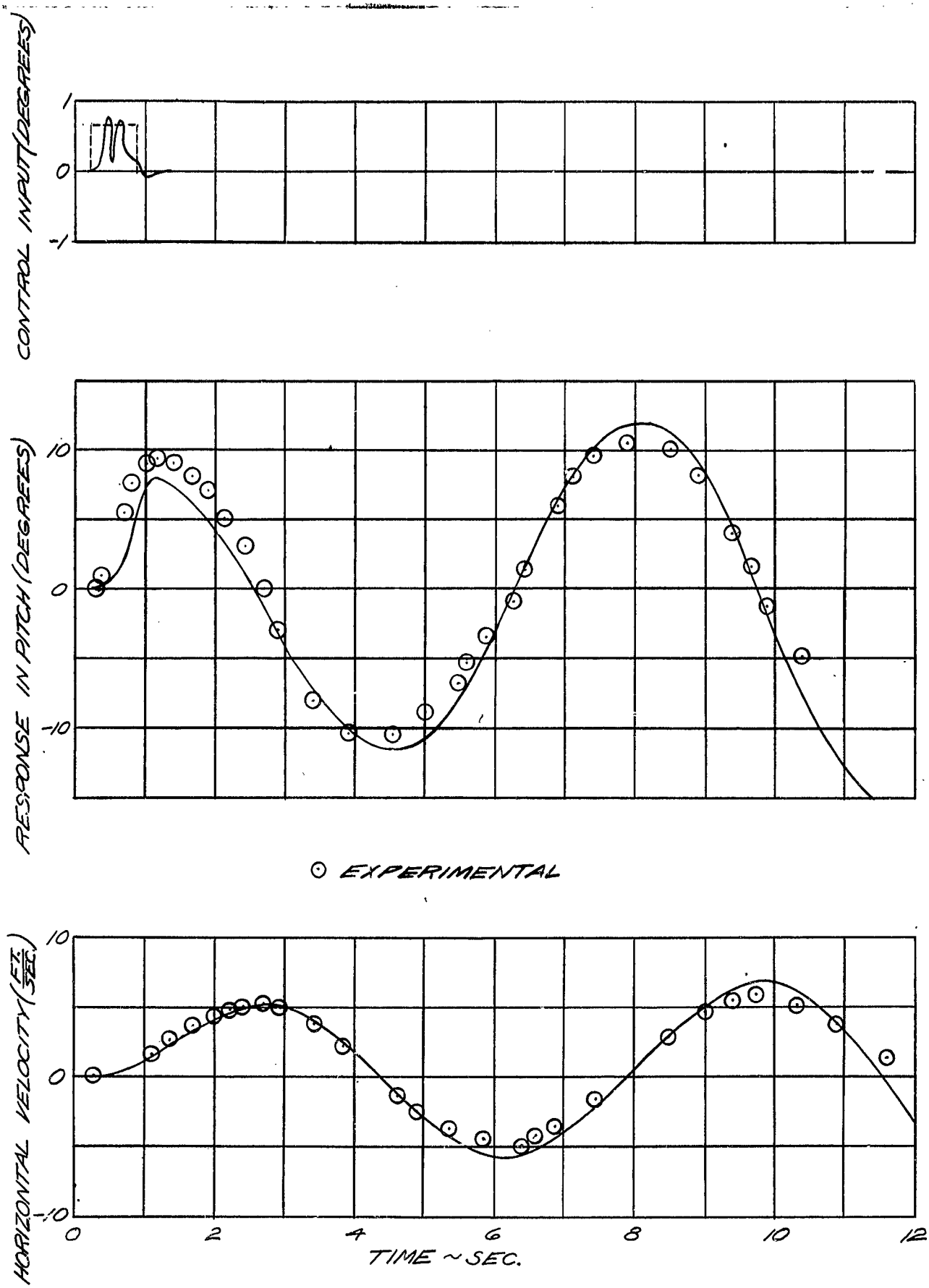

Fig. 15 Experimental and Theoretical Fuselage Response to a Step Disturbance - (Run 2-19-53)

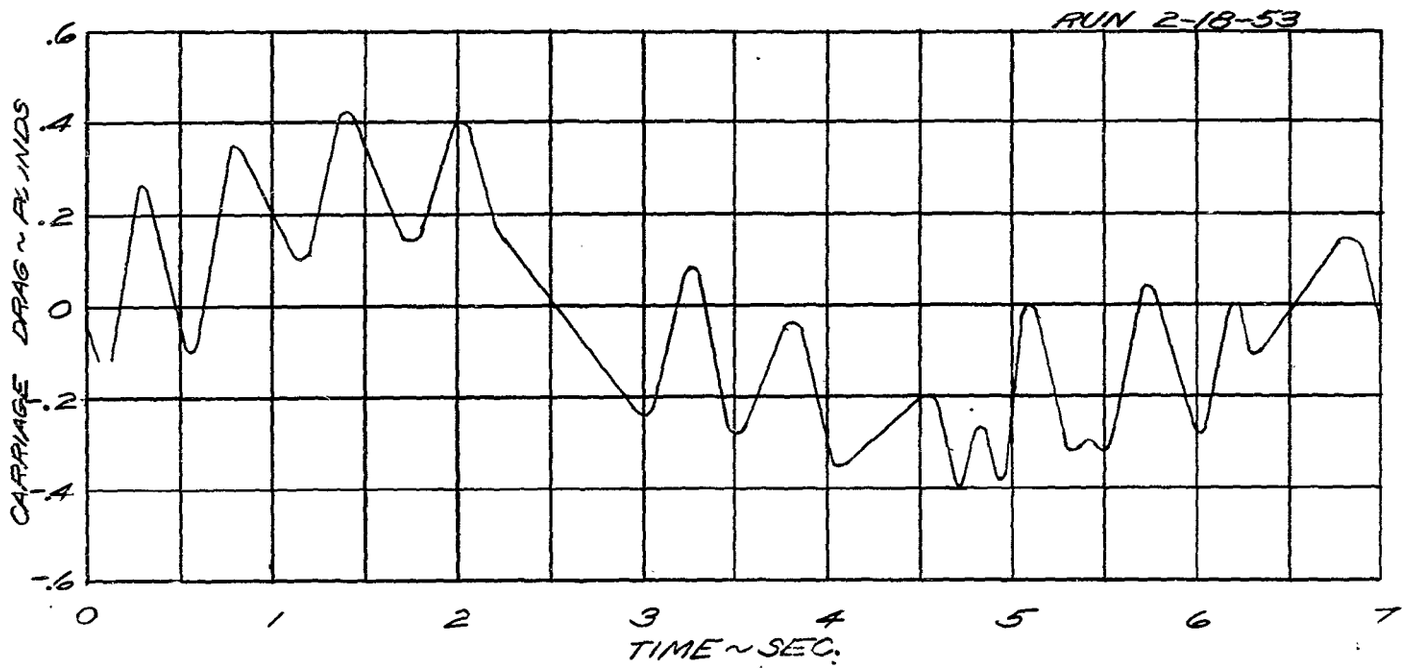

Fig. 16 Carriage Drag

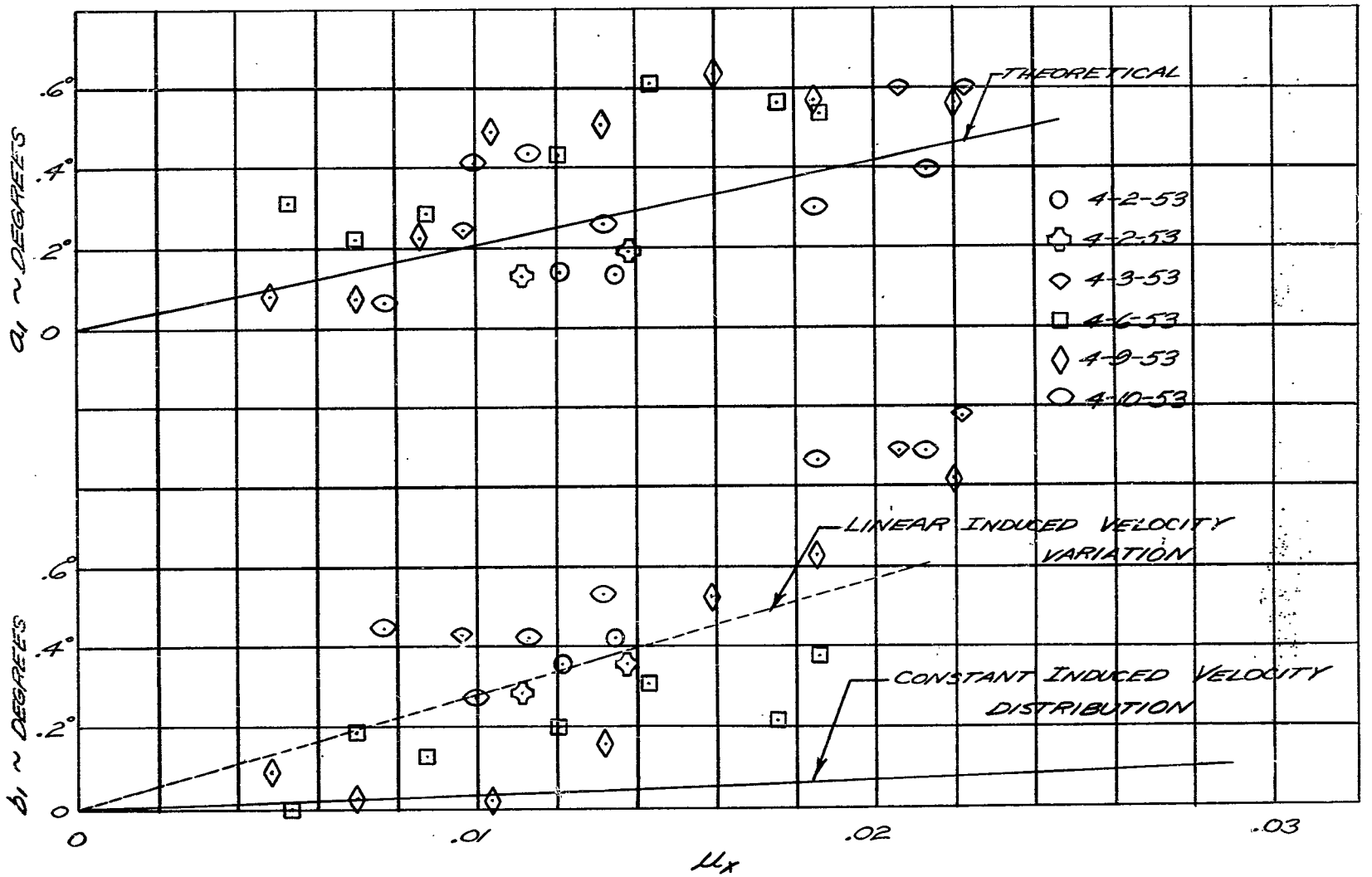

Fig. 17 Flapping Due to Forward Velocity

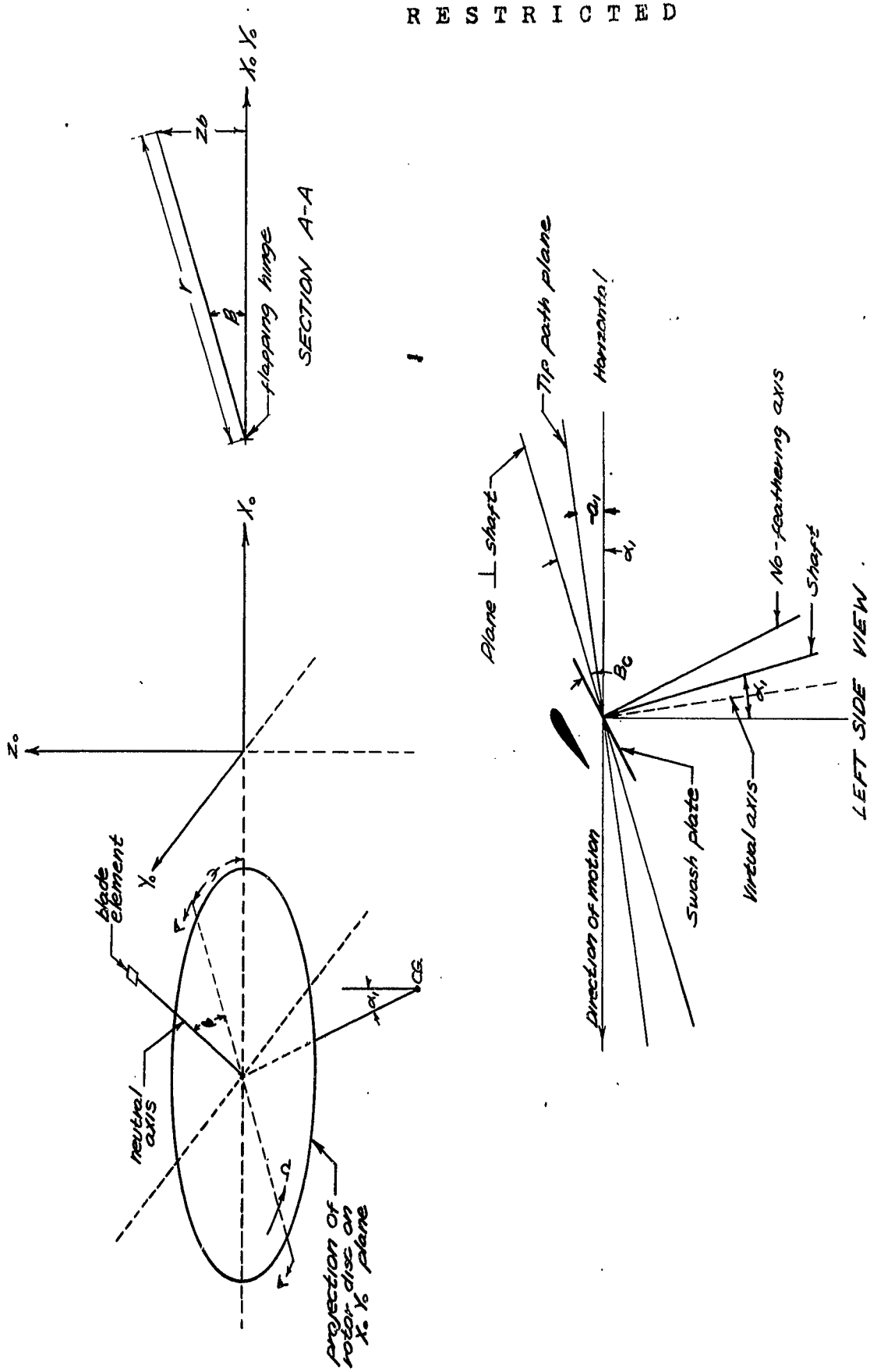

Fig. 18 Coordinate Axes